Electronic Supplementary Information

Carboxylic Acid Ligand Substituent Impacts Hydrosilylation Activity of Platinum Single Atom Catalysts on Ceria

Nicholas A. Maciulis,[a] Eman Wasim,[a] Fereshteh Rezvani,[a] Maren Pink,[a] George E. Sterbinsky,[b] Kenneth G. Caulton,[a] and Steven L. Tait[a,*]

[a] Department of Chemistry, Indiana University, 800 E. Kirkwood Ave., Bloomington, Indiana 47405 (U. S. A.).

* E-mail: tait@indiana.edu, Tel.: +1-812-855-1302.

[b] Advanced Photon Source, Argonne National Laboratory, 9700 S. Cass Ave., Lemont, Illinois 60439 (U. S. A.).

Contents

Discovery of decarboxylation reactivity of PDO-C2 by H_2PtCl_6.

Early experiments explored H_2PtCl_6 as platinum source, but coordination of PDO-C2 did not occur at room temperature. Heating PDO-C2 and H_2PtCl_6 at 80 °C in water/acetic acid mixture resulted in decarboxylation to afford PDO-C. Heating PDO-C2 at 80 °C in water in the absence of H_2PtCl_6 also leads to decarboxylation, ruling out metal induced decarboxylation. Further heating at higher temperatures and addition of excess H_2PtCl_6 did not lead to loss of remaining carboxylic acid group. XPS data indicates Pt(II) in the sample from reaction of PDO-C2 and H_2PtCl_6 in water; Pt(IV) is merely acting as an oxidant (Figure S1).

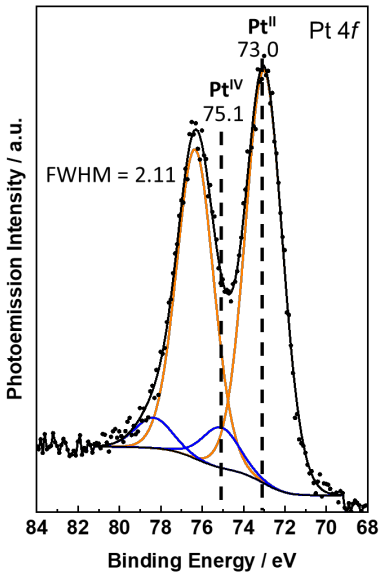

Fig. S1 Pt 4f XPS spectrum of sample from crystal that contains 3% impurity from reaction of H_2PtCl_6 + PDO-C2 in water heated at 80 °C for 12 hours. XPS spectrum was referenced against C1s (285 eV). Major Pt species at 73.0 eV is consistent with Pt(II) and the peak at 75.1 eV is consistent with Pt(IV) remaining H_2PtCl_6 in sample.

Characterization Data of PDO-C

Figures S2-S5 show the ^{1}H, ^{13}C NMR, and FTIR spectra for PDO-C. Figure S7 shows the crystal structure of the PDO-C ligand and PDO-C coordinated to Pt modeled as a 2% impurity in crystal structure of PDO-C:DMSO crystal structure.

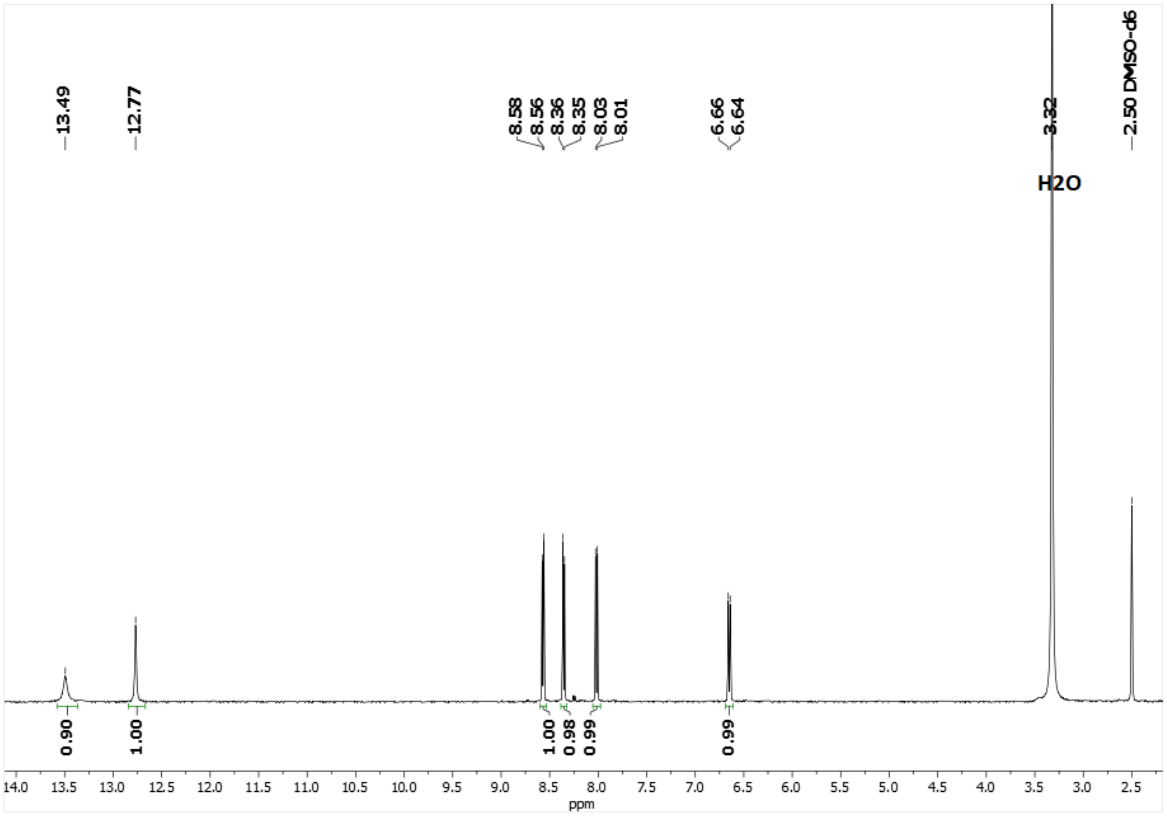

Fig. S2 ^{1}H NMR spectrum of PDO-C in DMSO-d_6.

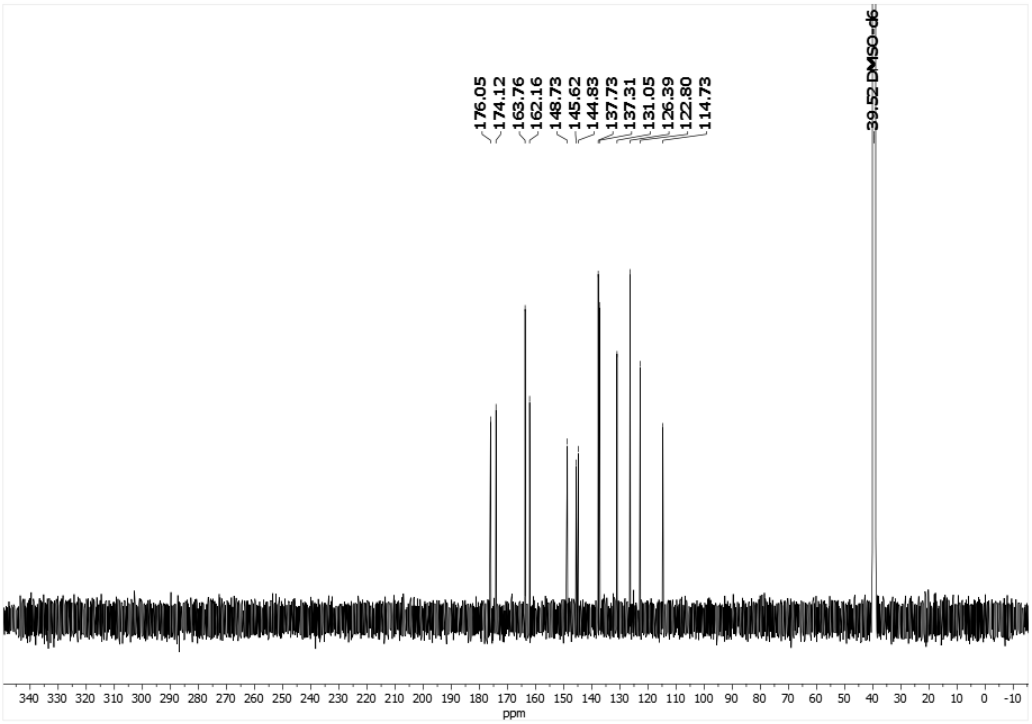

Fig. S3 ^{13}C NMR spectrum of PDO-C in DMSO-d_6.

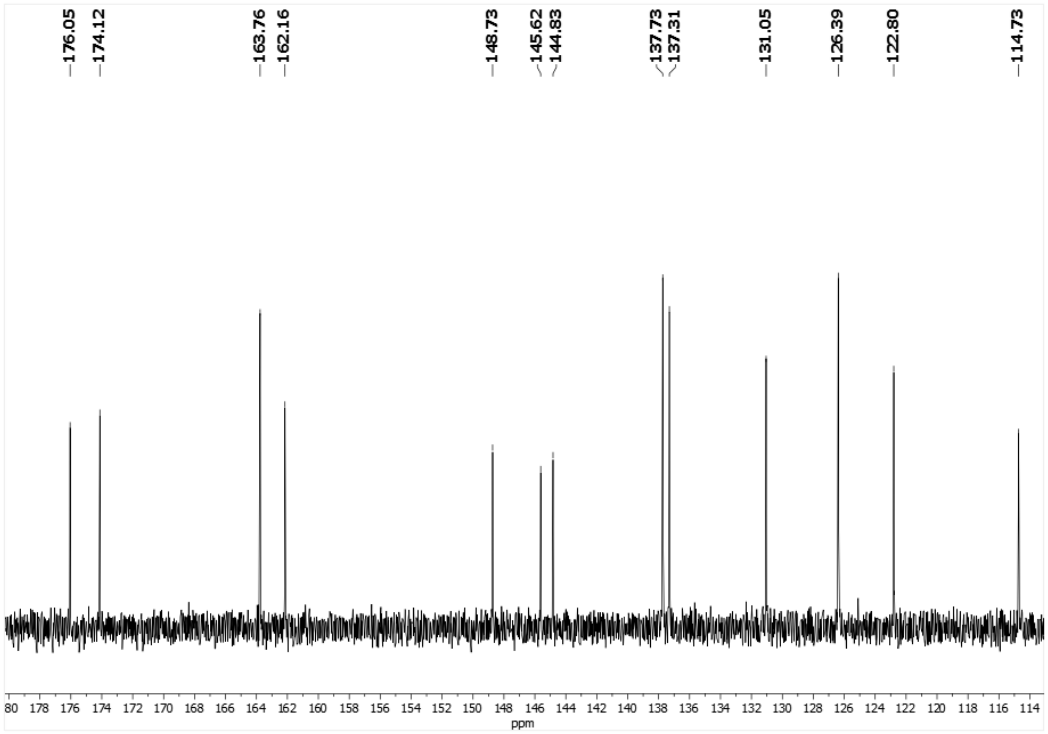

Fig. S4 Expansion of aromatic region in Fig. S3 ^{13}C NMR spectrum in DMSO-d_6.

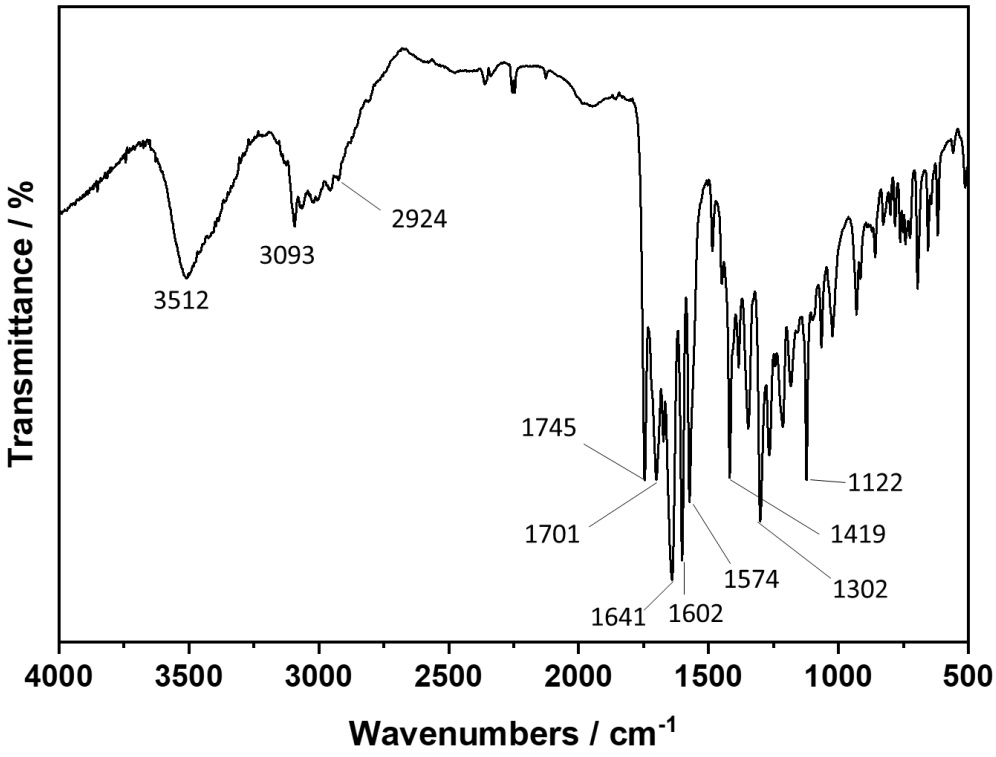

Fig. S5 FTIR spectrum in KBr of PDO-C.

X-ray Crystallographic Data collection of PDO-C

An orange crystal (approximate dimensions 0.192 × 0.261 × 0.279 mm^3) was placed onto the tip of a MiTeGen loop and mounted on a Bruker Venture D8 diffractometer equipped with a PhotonIII detector at 123(2) K.

The data collection was carried out using Mo Kα radiation (graphite monochromator) with a frame time of 1 or 1.5 seconds and a detector distance of 4.00 cm. A collection strategy was calculated and complete data to a resolution of 0.71 Å with a redundancy of 3.4 were measured. Nine major sections of frames and two fast scans were collected with 0.50° ω and ϕ scans. A total of 3438 frames were collected, and the total exposure time was 1.01 hours.

The frames were integrated with the Bruker SAINT software package [1]using a narrow-frame algorithm. The integration of the data using a monoclinic unit cell yielded a total of 78401 reflections to a maximum θ angle of 27.52° (0.77 Å resolution), of which 3356 were independent (average redundancy 23.361, completeness = 99.9%, R_{int} = 6.04%, R_{sig} = 1.75%) and 2861 (85.25%) were greater than $2\sigma(F^2)$. The final cell constants of a = 14.2283(5) Å, b = 12.4939(4) Å, c = 8.2937(2) Å, β = 98.4225(12)°, volume = 1458.44(8) $Å^3$, are based upon the refinement of the XYZ-centroids of 9780 reflections above 20 σ(I) with 5.789° < 2θ < 54.88°. Data were corrected for absorption effects using the Multi-Scan method (SADABS).[2] The ratio of minimum to maximum apparent transmission was 0.924. The calculated minimum and maximum

transmission coefficients (based on crystal size) are 0.8830 and 0.9180.

Structure solution and refinement

The space group $P2_1/c$ was determined based on intensity statistics and systematic absences. The structure was solved and refined using the SHELX suite of programs. [3, 4] An intrinsic-methods solution was calculated, which provided most non-hydrogen atoms from the E-map. Full-matrix least squares / difference Fourier cycles were performed, which located the remaining non-hydrogen atoms. All non-hydrogen atoms were refined with anisotropic displacement parameters. The hydrogen atoms were placed in ideal positions and refined as riding atoms with relative isotropic displacement parameters. The structure was found as a co-crystal of protonated ligand × solvent and PtClLig. Overlapping atom sites were refined with restraints and constraints.

The final anisotropic full-matrix least-squares refinement on F2 with 234 variables converged at R1 = 3.85%, for the observed data and wR2 = 9.86% for all data. The goodness-of-fit was 1.042. The largest peak in the final difference electron density synthesis was 0.347 e-/Å^3 and the largest hole was -0.462 e-/Å^3 with an RMS deviation of 0.051 e-/Å^3. On the basis of the final model, the calculated density was 1.600 g/cm^3 and F(000), 724 e-. Hydrogen bonding was found between the protonated ligand and DMSO.

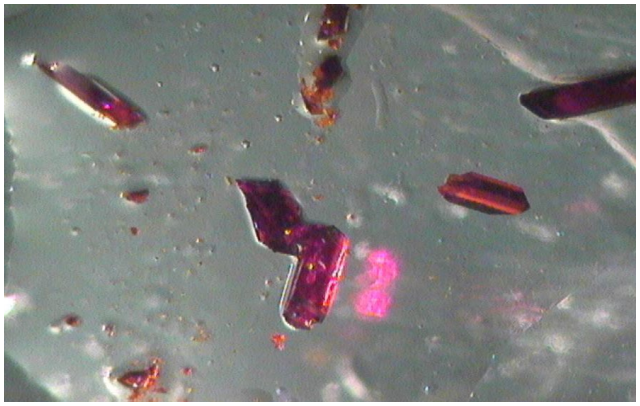

Fig. S6 Picture of Bulk material.

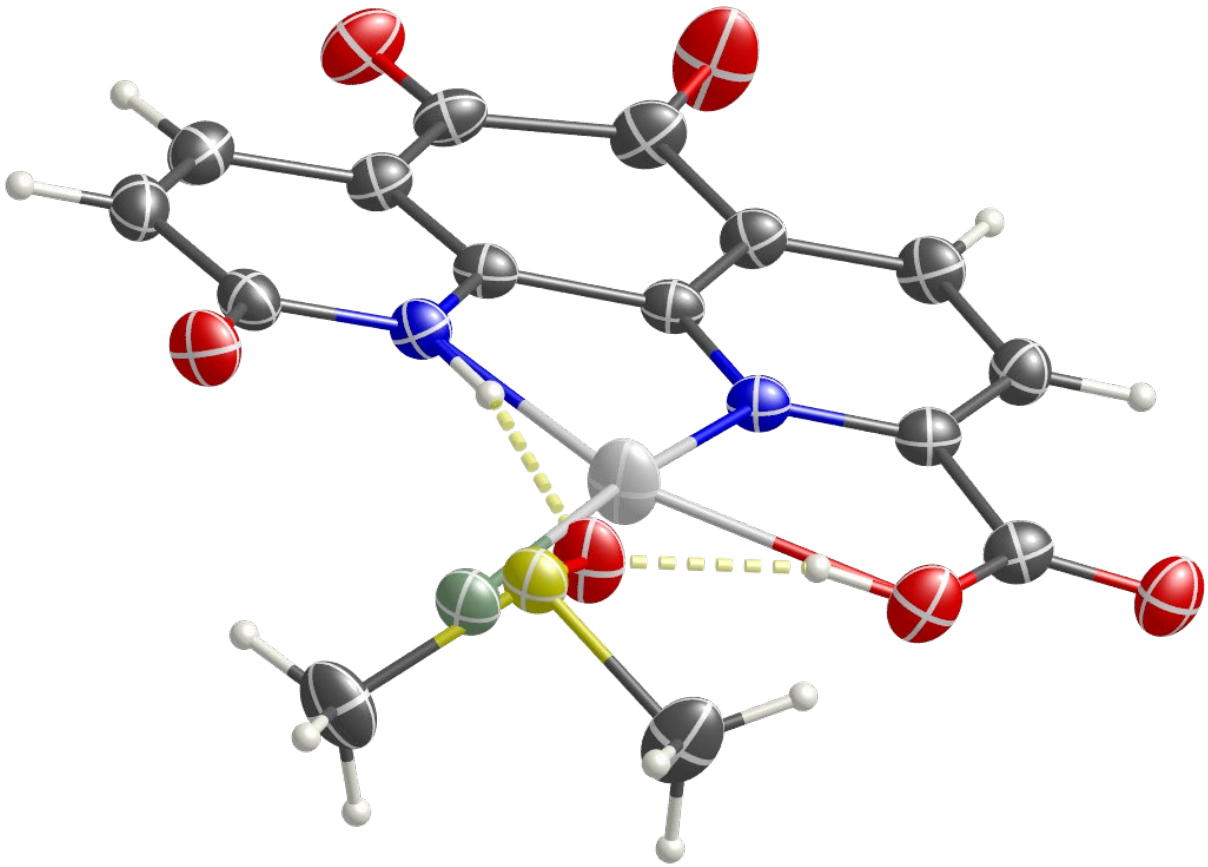

Fig. S7 Co-crystal disorder, ellipsoids at 50% probability level.

Table S1 Crystal data and structure refinement for 0.98 ($C_{13}H_6N_2O_5$, $OS(CH_3)_2$ × 0.02 $PtCl(C_{13}H_4N_2O_5)$ co-crystal.

Empirical formula	C14.96 H11.84 Cl0.02 N2 O5.98 Pt0.02 S0.98	
Formula weight	351.40	
Crystal color, shape, size	dark orange block, 0.279 × 0.261 × 0.192 mm^3	
Temperature	123(2) K	
Wavelength	0.71073 Å	
Crystal system, space group	Monoclinic, $P2_1/c$	
Unit cell dimensions	a = 14.2283(5) Å	α = 90°.
	b = 12.4939(4) Å	β = 98.4225(12)°.
	c = 8.2937(2) Å	γ = 90°.

Volume	1458.44(8) $Å^3$
Z	4
Density (calculated)	1.600 Mg/m^3
Absorption coefficient	0.455 mm^{-1}
F(000)	724

Data collection

Diffractometer	Venture D8, Bruker
Source	IμS 3.0, Incoatec
Theta range for data collection	2.180 to 27.520°.
Index ranges	-18<=h<=18, -16<=k<=16, -10<=l<=10
Reflections collected	78401
Independent reflections	3356 [R_{int} = 0.0604]
Observed Reflections	2861
Completeness to theta = 25.242°	99.9 %

Solution and Refinement

Absorption correction	Semi-empirical from equivalents
Max. and min. transmission	0.7456 and 0.6887
Solution	Intrinsic methods
Refinement method	Full-matrix least-squares on F^2
Weighting scheme	$w = [\sigma^2 Fo^2 + 0.0419P^2 + 1.0894P]^{-1}$, with $P = (Fo^2 + 2\,Fc^2)/3$
Data / restraints / parameters	3356 / 0 / 234
Goodness-of-fit on F^2	1.042
Final R indices [I>2□(I)]	R1 = 0.0385, wR2 = 0.0930
R indices (all data)	R1 = 0.0480, wR2 = 0.0986
Largest diff. peak and hole	0.347 and -0.462 $e.Å^{-3}$

Goodness-of-fit = $[\Sigma[w(F_o^2 - F_c^2)^2]/N_{observns} - N_{params})]^{1/2}$, all data.

$R1 = \Sigma(|F_o| - |F_c|) / \Sigma |F_o|$. $wR2 = [\Sigma[w(F_o^2 - F_c^2)^2] / \Sigma [w(F_o^2)^2]]^{1/2}$.

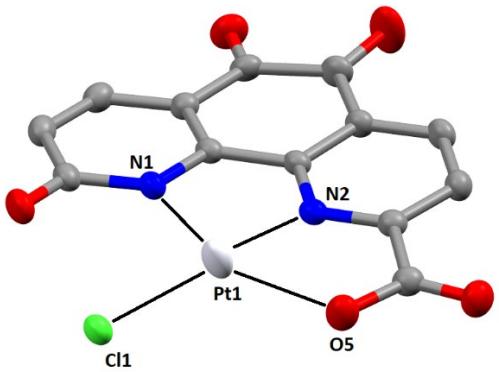

Fig. S8 Connectivity of co-crystal structure of Pt(Cl)-PDO-C with hydrogens removed for clarity; relevant distances (Å) and angles (°) are as follows: N1-Pt1, 2.185(4); N2-Pt1, 1.966(4); O5-Pt1, 2.488(4); Pt1-Cl1, 2.62(3); ∠N2-Pt1-N1, 80.83(13); ∠N1-Pt1-Cl1, 104.2(6); ∠N2-Pt-O5, 73.30(13); ∠O5-Pt1-Cl1, 101.7(6).

Catalytic Activity of Pt/Ligand/CeO_2 prepared in acetonitrile, where Ligand = PDO, PDO-C, and PDO-C2

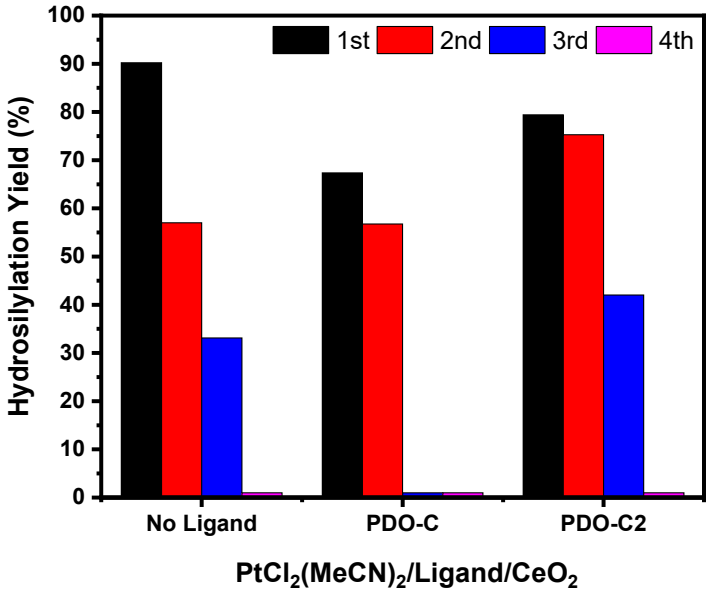

Fig. S9 Comparison of hydrosilylation yields for four consecutive runs using three heterogeneous catalysts $PtCl_2(MeCN)_2$/Ligand/CeO_2, where Ligand = No Ligand, PDO-C, PDO-C2 prepared by stirring ligand with ceria for 1.5 hours in acetonitrile followed by addition of $PtCl_2(MeCN)_2$ in acetonitrile dropwise over ten minutes and stirring for 12 hours. Originally, the synthesis of the heterogeneous catalysts used acetonitrile

as solvent due to improved solubility of $PtCl_2(MeCN)_2$, but due to poor recyclability of catalyst water was explored as a solvent.

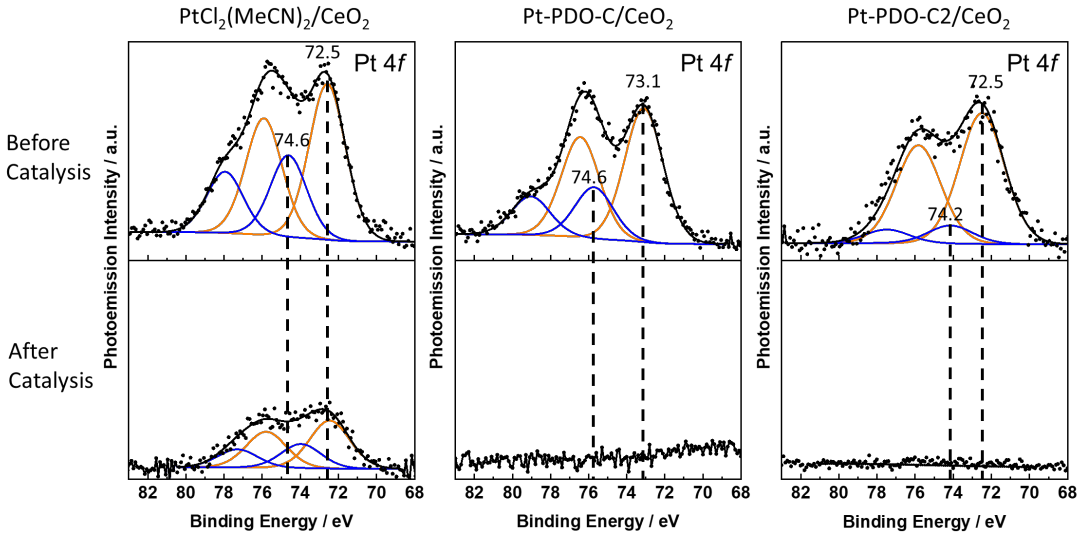

Fig. S10 Pt 4f XPS spectra for before (above) and after (below) 4 cycles of catalysis for three heterogeneous catalysts $PtCl_2(MeCN)_2$/Ligand/CeO_2, where L = No Ligand, PDO-C, and PDO-C2.

Table S2 Platinum loading before and after catalysis for Pt(II)/Ligand/CeO_2 prepared in acetonitrile.

	No Ligand	PDO-C	PDO-C2
% Pt Loading Before Catalysis	0.10	0.20	0.094
% Pt Loading After Catalysis	0.061	0.083	0.021

XPS spectra comparison of $PtCl_2(MeCN)_2/CeO_2$ and Pt/Ligand/CeO_2 prepared using synthetic methods 1 and 2

Fig. S11-S16 are stacked Pt 4f, O 1s, N 1s, Cl 2p, and C 1s spectra for comparison of $PtCl_2(MeCN)_2/CeO_2$ and CeO_2 to synthetic method 1 and 2 of Pt/Ligand/CeO_2 and CeO_2, where Ligand = PDO, PDO-C, and PDO-C2. Unless otherwise noted, XPS spectra were vertically scaled to show comparison of peak shape and weaker signals.

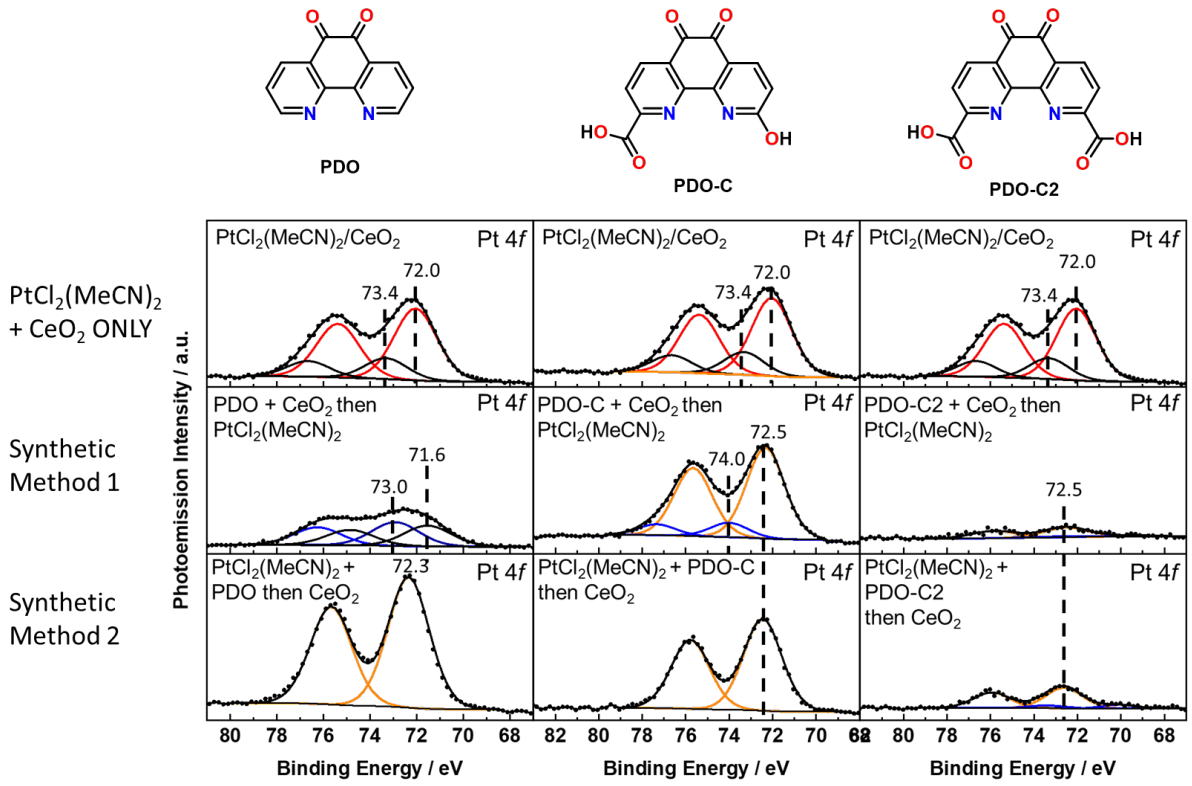

Fig. S11 Pt 4f XPS spectra of $PtCl_2(MeCN)_2/CeO_2$ (top), Method 1 (middle), and Method 2 (bottom) normalized by Ce 3d peak height.

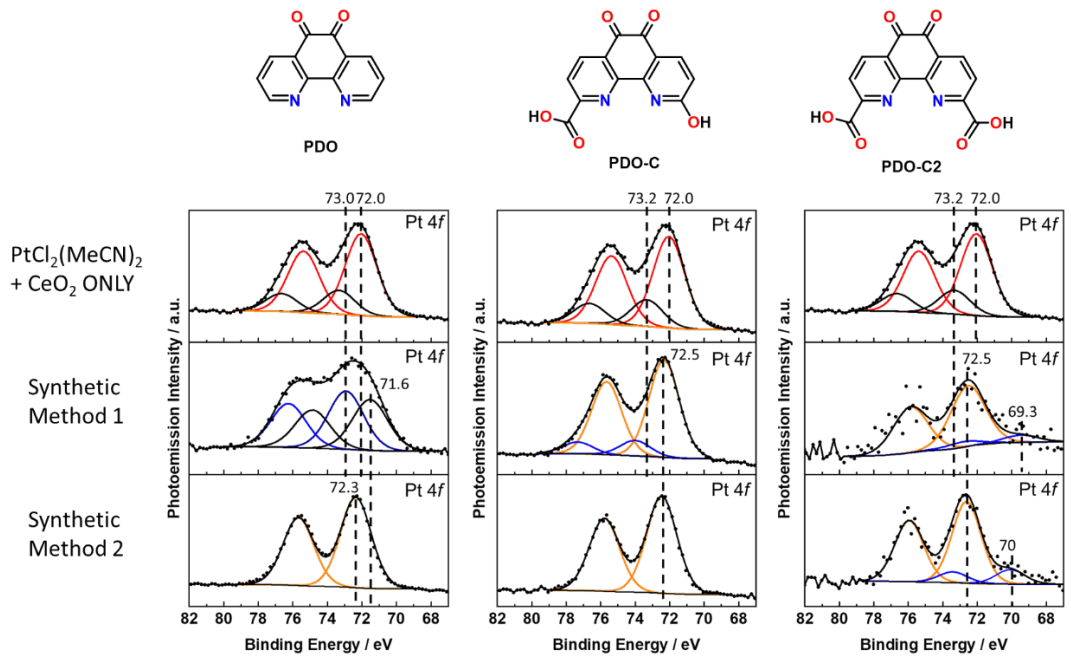

Fig S12 Pt 4f XPS spectra of $PtCl_2(MeCN)_2/CeO_2$ (top), Method 1 (middle), and Method 2 (bottom).

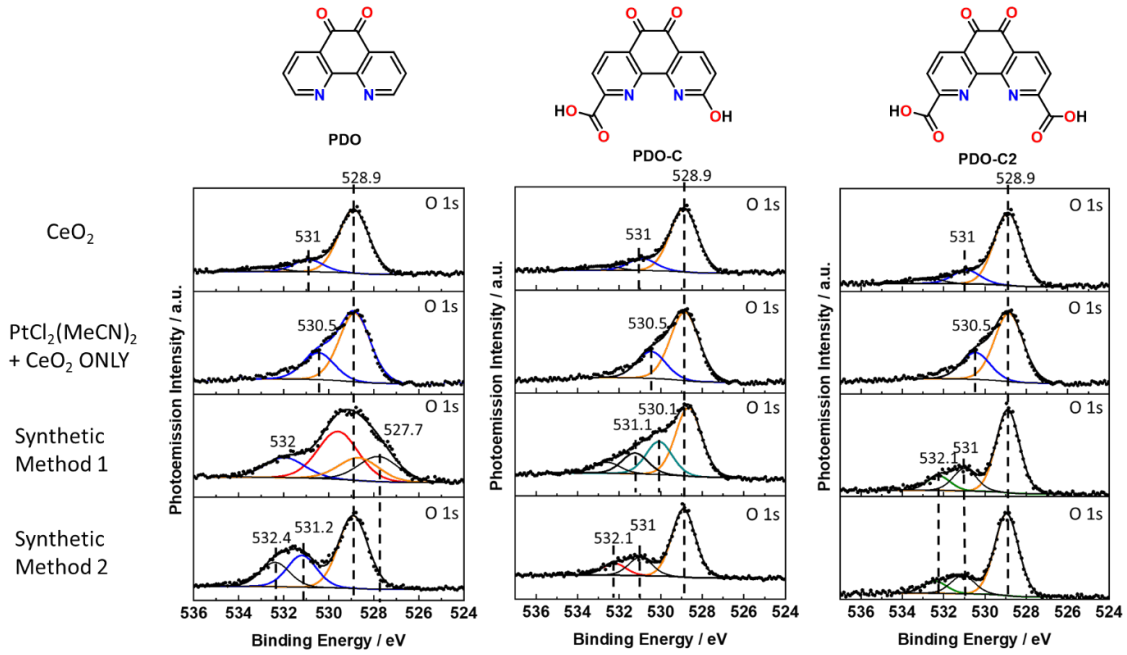

Fig. S13 O 1s XPS spectra of CeO_2, $PtCl_2(MeCN)_2/CeO_2$ ONLY, Method 1, and Method 2 (top to bottom).

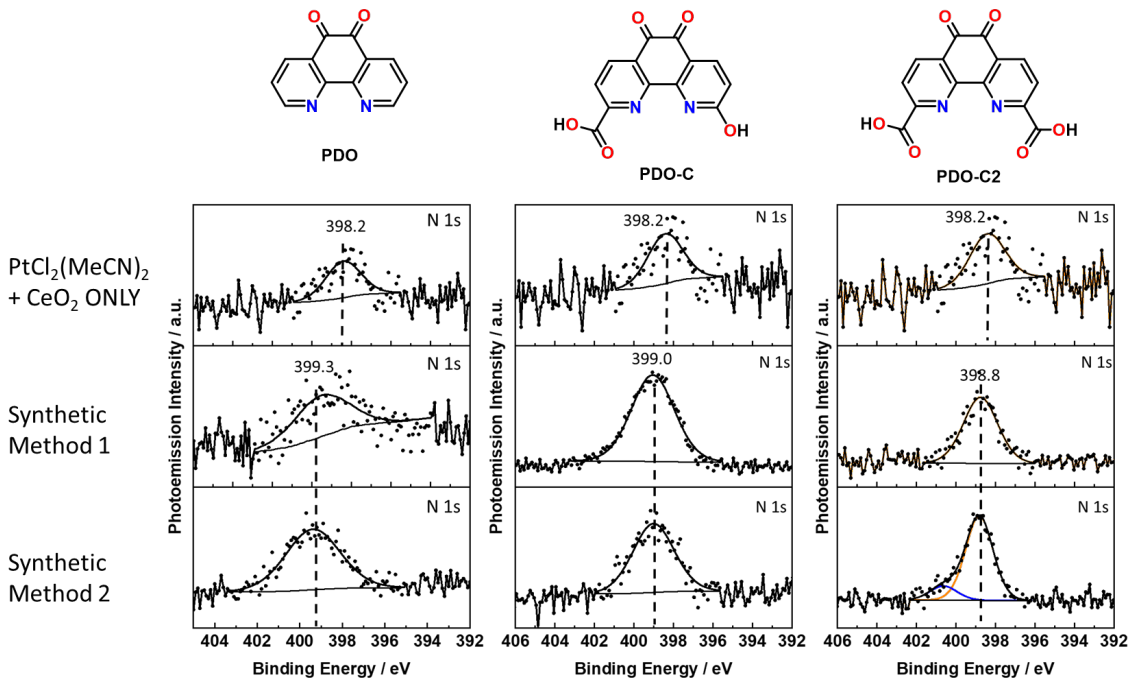

Fig. S14 N 1s XPS spectra of $PtCl_2(MeCN)_2/CeO_2$ ONLY, Method 1, and Method 2 (top to bottom).

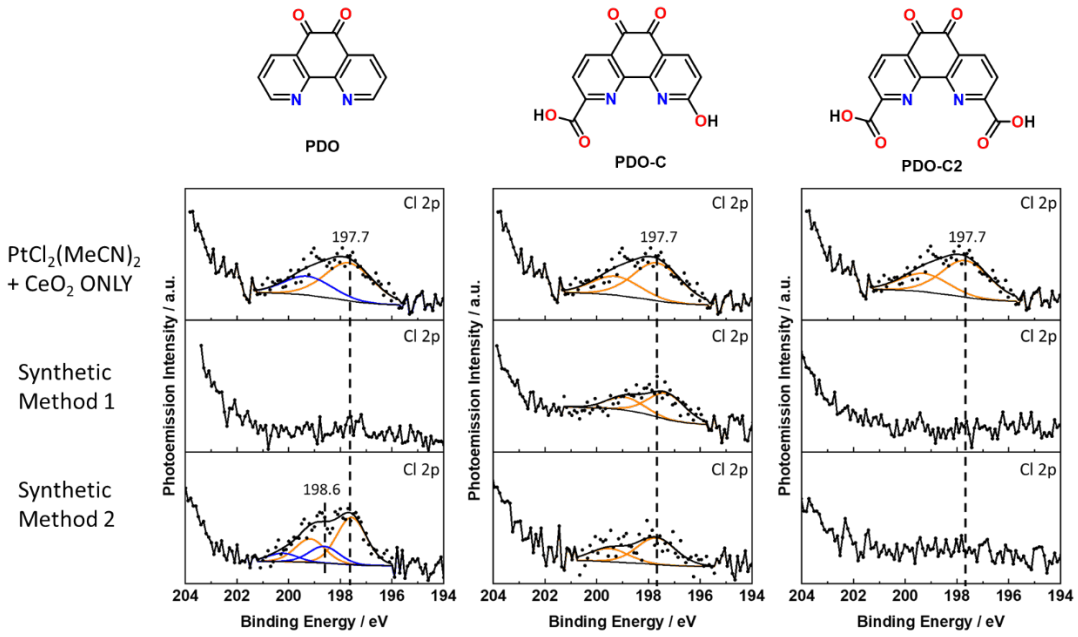

Fig. S15 Cl 2p XPS spectra of $PtCl_2(MeCN)_2/CeO_2$ without Ligand, Method 1, and Method 2 (top to bottom).

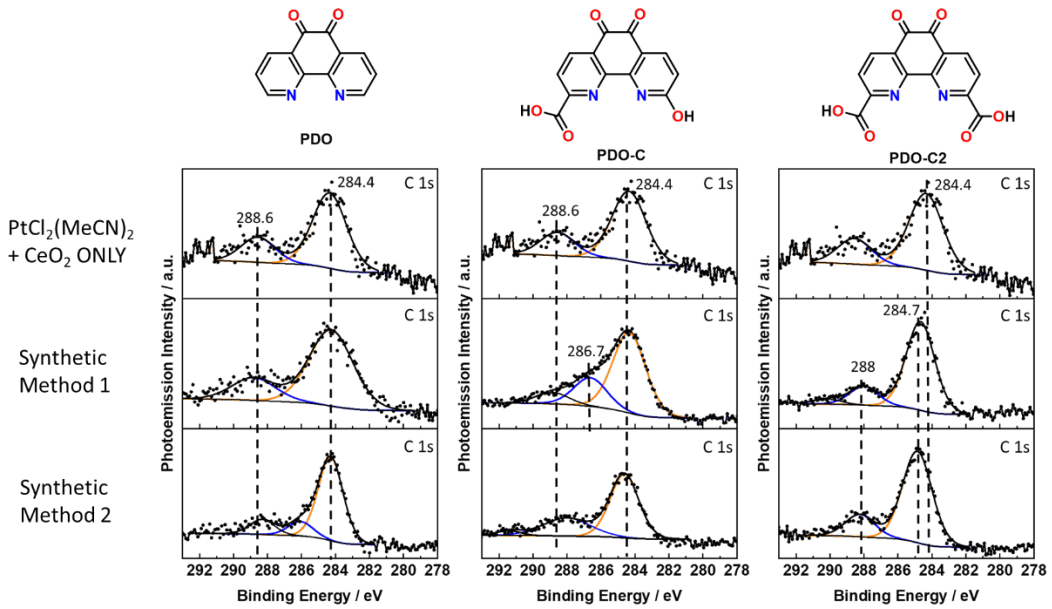

Fig. S16 C 1s XPS spectra of $PtCl_2(MeCN)_2/CeO_2$ ONLY, Method 1, and Method 2 (top to bottom).

Understanding ligand loading on ceria surface with and without platinum using Method 2

Fig. S17 shows the N 1s spectra comparison of Ligand + CeO2 and Pt/Ligand/CeO_2 using synthetic Method 2. Changes in FWHM and binding energy were used to support SAC on surface or mostly Ligand on ceria surface. Table S2 shows the element ratios further support more SAC on ceria for Pt/Ligand/CeO_2 when Ligand is PDO and PDO-C, than when Ligand is PDO-C2.

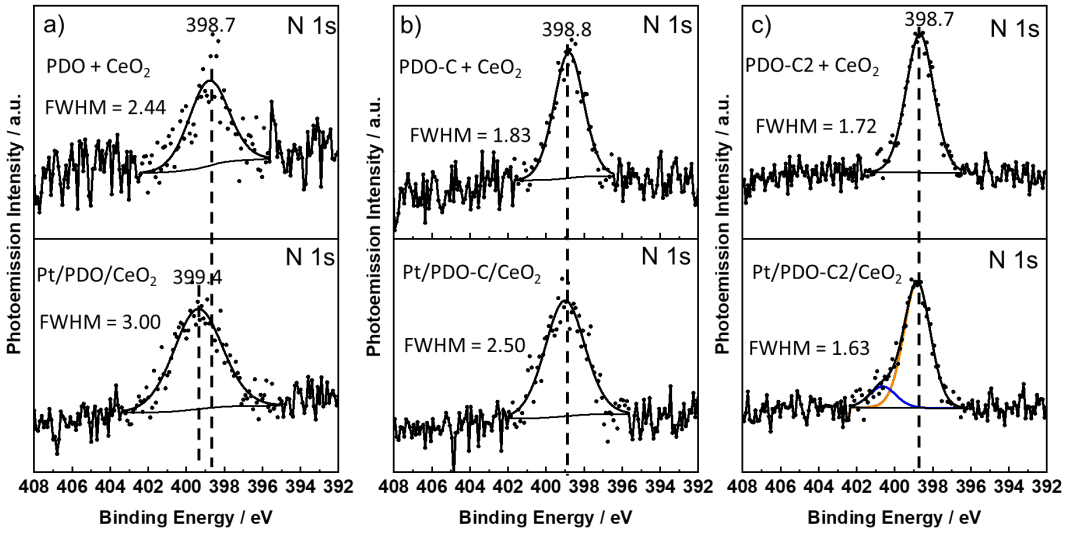

Fig. S17 Comparison of N 1s BE and FWHM of Ligand/CeO_2 versus Pt/Ligand/CeO_2, where Ligand = PDO (a), PDO-C (b), and PDO-C2 (c).

Table S3 Comparison of XPS Element Ratios of Ligand/CeO_2 and Pt/Ligand/CeO_2 synthesized by Method 2. [a]0.046 mmol of Ligand was allowed to stir with 0.300 g CeO_2 for 12 hours in deionized water before washing with deionized water and acetonitrile (three times each).

Catalyst	***Cl:Pt***	***N:Pt***	***Pt:Ce***	***N:Ce***
PDO/CeO_2[a]	-	-	-	0.38
PDO-C/CeO_2[a]	-	-	-	0.91
PDO-C2/CeO_2[a]	-	-	-	1.32
Pt-PDO/CeO_2	0.75	1.30	0.68	0.88
Pt-/PDO-C/CeO_2	0.69	3.05	0.37	1.11
Pt-/PDO-C2/CeO_2	0.00	14.8	0.098	1.44

Steric Models

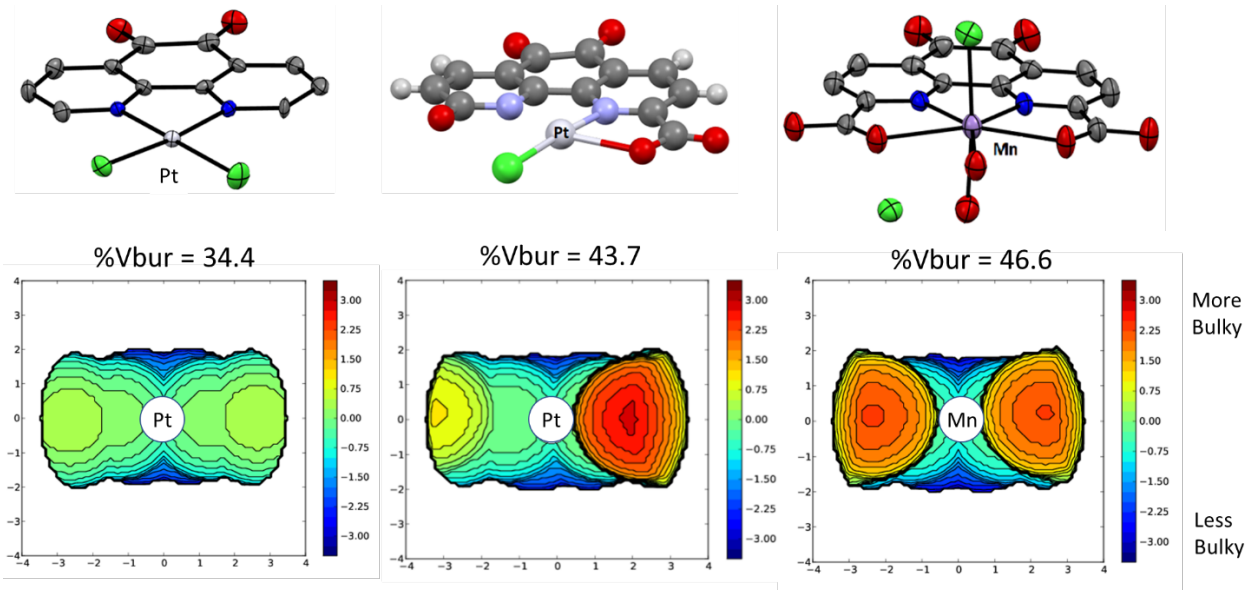

Fig. S18 Topographic steric maps and percent buried volume[5] (%Vbur) of PDO, PDO-C, and PDO-C2 (left to right) viewed down the bisector of the bidentate ligand angle, ∠N-M-N. The platinum or manganese atom was set as the center of coordination sphere and the radius of the sphere was set to 3.5 Å for topographic map and %Vbur calculations. The crystallographic data for Pt-PDO[6] and Mn-PDO-C2[7] were obtained from published data. Red regions show greater steric bulk arising from ligand oxygens, with manganese example included to show further congestion from two carboxylates. Percent buried volume reinforces this conclusion but evaluated by a global parameter. https://www.molnac.unisa.it/OMtools/sambvca2.1/index.html

Investigation of Ligand Coordination: SAC complex formation in solution

Control reactions to see if Ligand + $PtCl_2(MeCN)_2$ in water, where Ligand = PDO, PDO-C, and PDO-C2, forms a complex in water. A vial equipped with a stir bar was loaded with 0.046 mmol of Ligand and 0.016 g $PtCl_2(MeCN)_2$ (0.046 mmol) followed by addition of 10 mL of deionized water. The reactions stirred for 12 hours at room temperature. When Ligand is PDO, the solution turns blue. For PDO-C, the solution has a faint orange color. For PDO-C2, the solution is colorless. All solutions remain heterogeneous. Since the PDO-C and PDO-C2 are poorly soluble in water, the reaction solution was centrifuged and the mother liquor was decanted. The wet solid at bottom of vial was placed under vacuum to remove water and the samples were dissolved in DMSO-d_6. The ^{1}H NMR spectra of reaction of Ligand + $PtCl_2(MeCN)_2$ compared to Ligand are shown in Fig. S19-21. The ^{1}H NMR spectrum of $PtCl_2(MeCN)_2$ in DMSO-d_6 is provided in Fig. S22.

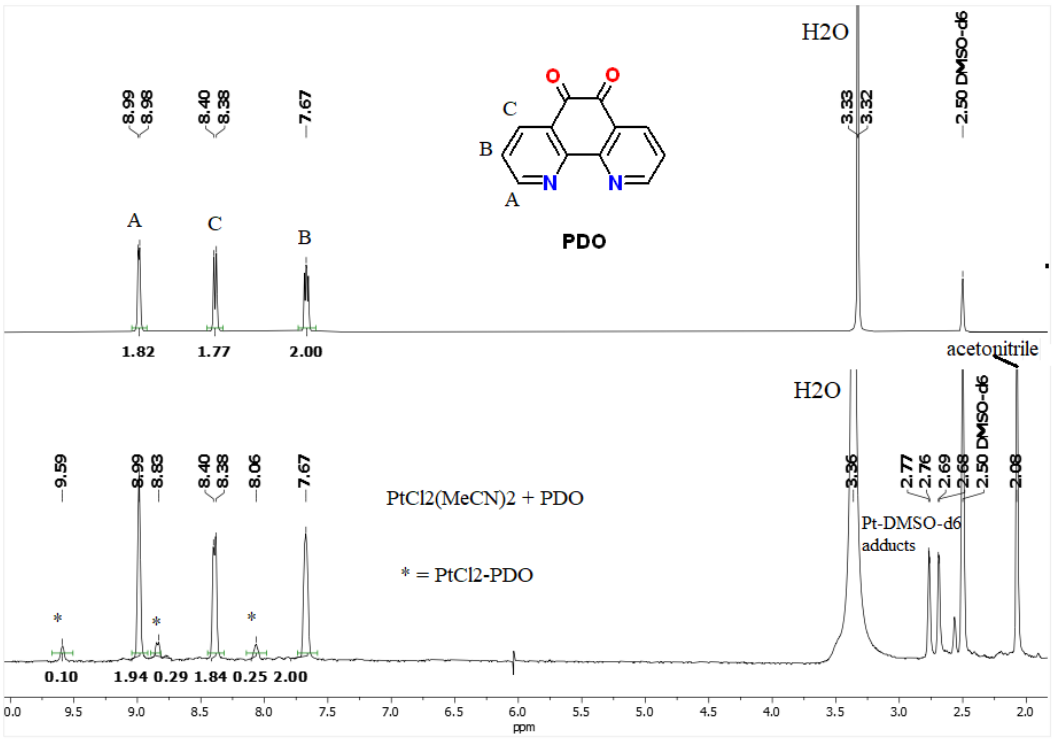

Fig. S19 Stacked ^{1}H NMR of PDO (top) and PDO + $PtCl_2(MeCN)_2$ (bottom) in DMSO-d_6.

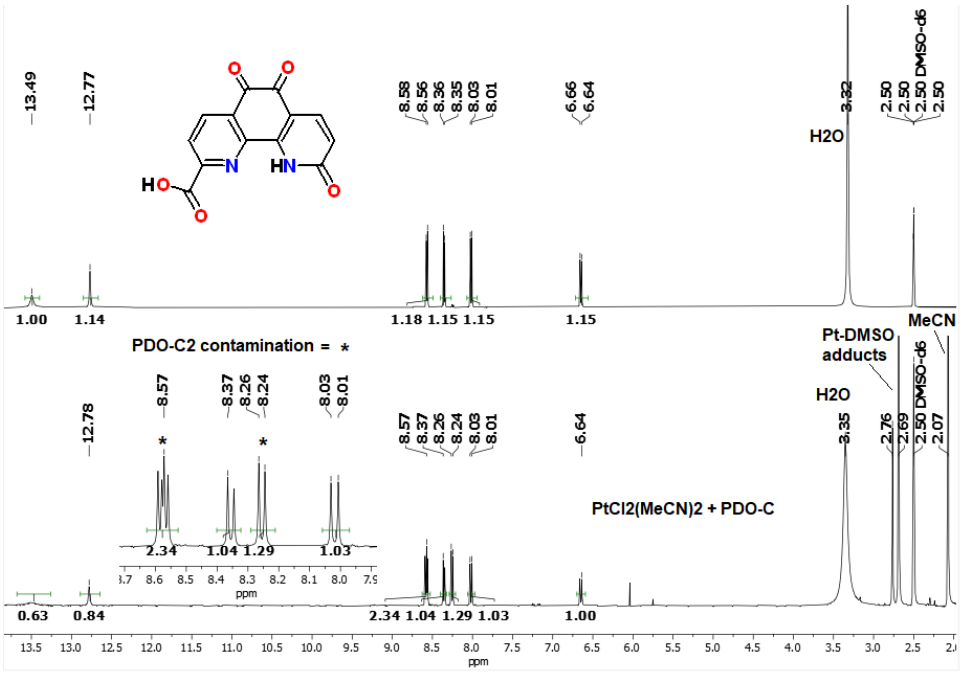

Fig. S20 Stacked ^{1}H NMR of PDO-C (top) and PDO-C + $PtCl_2(MeCN)_2$ (bottom) in DMSO-d_6.

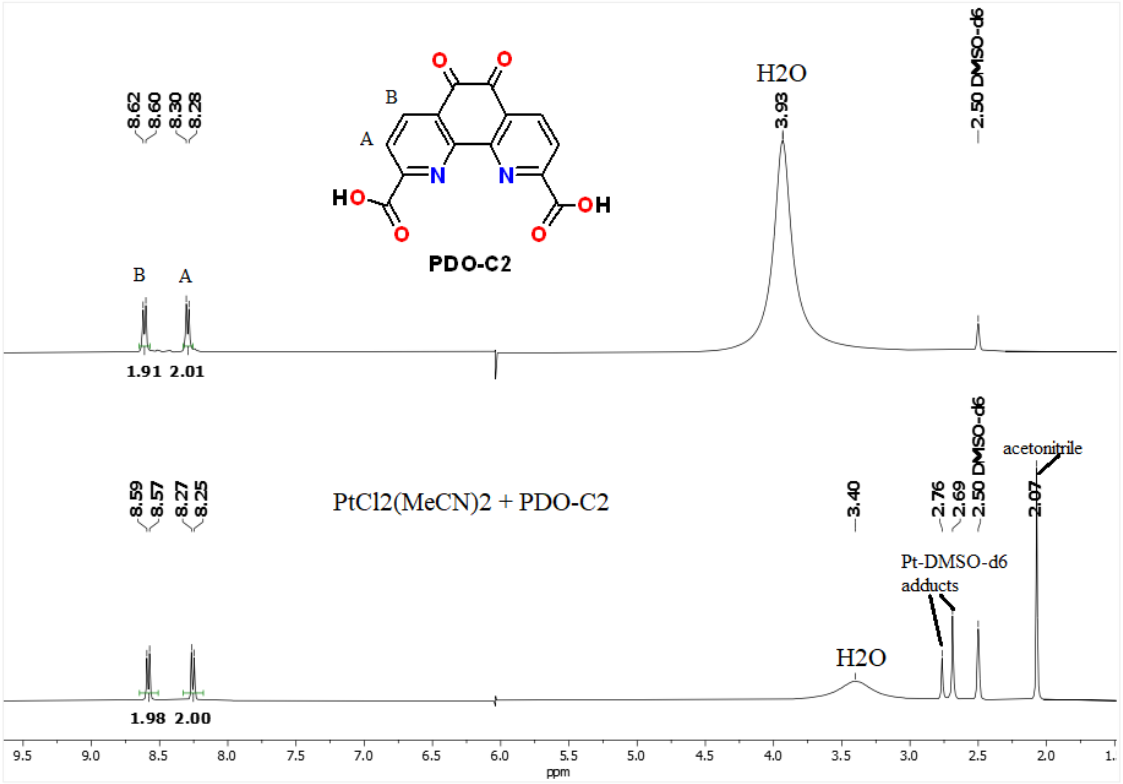

Fig. S21 Stacked ^{1}H NMR of PDO-C2 (top) and PDO-C2 + $PtCl_2(MeCN)_2$ (bottom) in DMSO-d_6.

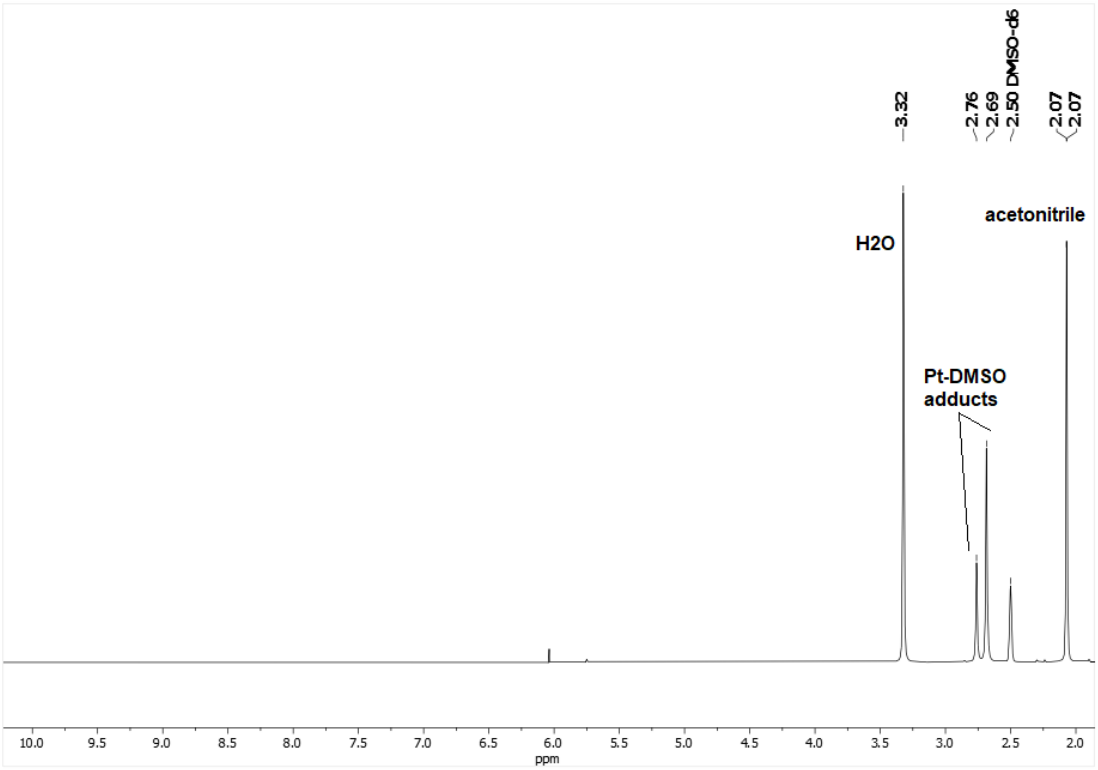

Fig. S22 ^{1}H NMR spectrum of $PtCl_2(MeCN)_2$ in DMSO-d_6.

Interaction of Pt-Ligand Catalyst with Surface

In the case of PDO on ceria (Figure S23), the terminal hydroxy group at 3700 cm^{-1} disappears and a ketone stretch at 1690 cm^{-1} appears increasing with increased concentration of PDO. The dione of PDO can undergo hydration under acidic or basic conditions to generate an alpha-hydroxy ketone[8, 9] that could bind to ceria but our reaction conditions for the catalyst synthesis are near neutral pH and the ketone stretch is still observable by DRIFTS, so we reject occurrence of this. The nitrogens of PDO and phenanthroline are known to act as bases, and hydrogen bonding can broaden and shift O-H to lower frequencies to explain the disappearance of the terminal hydroxy peak. A proposed surface interaction of PDO with ceria appears in Fig. S23, **c**.

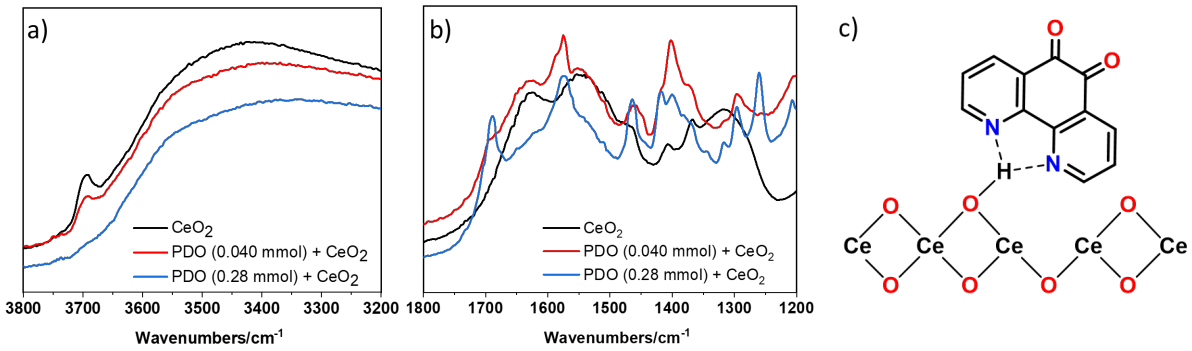

Fig. S23 DRIFT spectra for ceria (black), PDO + CeO_2 in H_2O (red), and excess PDO + CeO_2 (blue) in H_2O a) 3800-3200 cm^{-1} region b) 1800-1200 cm^{-1} region c) proposed hydrogen bonding of ligand to surface hydroxy group.

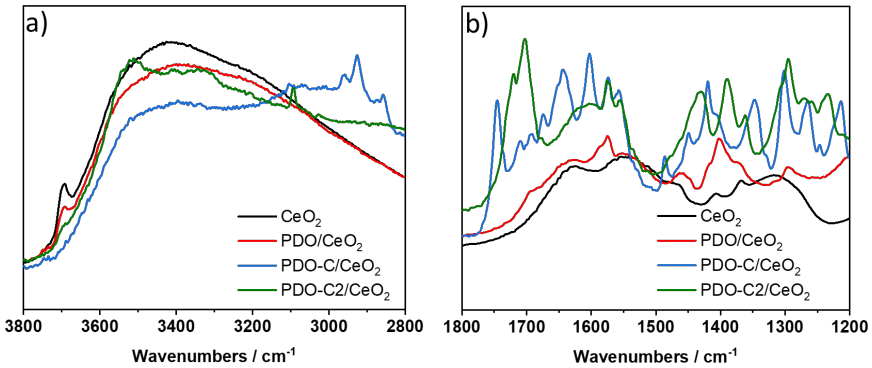

Fig S24 DRIFTS spectra of CeO_2 (black) and reaction of CeO_2 with PDO (red), PDO-C (blue), and PDO-C2 (green)

DRIFTS spectra collected on catalysts prepared by synthetic method 2 (Pt + PDO, then CeO_2) are shown in Figure S24. The terminal hydroxy peak at 3700 cm^{-1} disappears upon reaction of $PtCl_2(MeCN)_2$ and $PtCl_2(MeCN)_2$/PDO with ceria. The XPS ratio of Pt:Cl for all Pt(II)/Ligand/CeO_2 catalysts prepared in this study is less than 1:1. This suggests that the chemisorption of $PtCl_2(MeCN)_2$ and $PtCl_2(MeCN)_2$/PDO onto the surface involves at least one chloride exchange with surface hydroxy to form Pt-O bond and concomitant loss of HCl.

The absorbance at 2965 cm^{-1} corresponds to CH_3 proving acetonitrile is present on the surface. A shoulder at 1706 cm^{-1} appears in the DRIFTS spectrum of $PtCl_2(MeCN)_2$/PDO/CeO_2 (Fig. S25, red trace) corresponding to C=O stretch of dione that is blueshifted from PDO/CeO_2 (Fig. S24). The peak at 1264 cm^{-1} is also associated with impregnated solid. We interpret this as a Pt(II)/PDO complex that has deposited on the surface. One possible structure for SAC Pt(II)/PDO/CeO_2 is depicted in Fig. S25.

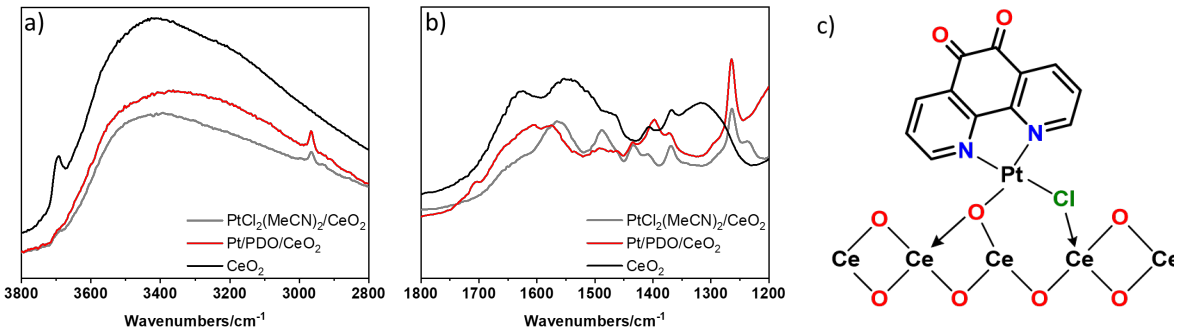

Fig. S25 DRIFTS spectra for CeO_2 (black), $PtCl_2(MeCN)_2/CeO_2$ (silver), and $PtCl_2(MeCN)_2/PDO/CeO_2$ (red) prepared in water a) 3800-2800 cm^{-1} region b) 1800-1200 cm^{-1} region and c) proposed structure on surface for $Pt(II)/PDO/CeO_2$.

Comparison of DRIFTS spectra for $Pt(II)/Ligand/CeO_2$, where Ligand = PDO, PDO-C, and PDO-C2, is shown in Fig. 3. DRIFT spectra show that the preferred site for binding catalyst to surface is the terminal hydroxy site. Peaks appearing from 3000-3100 cm^{-1} indicate aromatic C-H groups and ketone stretches at 1744-1708 cm^{-1} suggest that PDO-C and PDO-C2 are on surface. The intensity of the peaks for catalysts using substituted PDO ligands is more intense than PDO, suggesting a higher ligand loading on surface for PDO ligands containing anchoring groups. This is consistent with larger N:Ce XPS ratios for PDO-C and PDO-C2 than PDO deposited on ceria (Table S3).

Binding of carboxylic acids demonstrated by comparison to trimesic acid (TMA) and 4-fluorobenzoic acid.

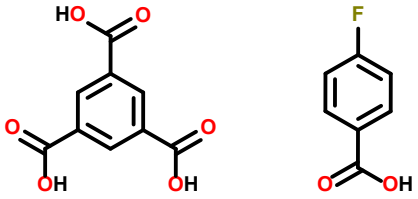

Scheme S1 Trimesic acid (left) and 4-fluorobenzoic acid (right).

XPS data was collected on CeO_2 that was treated with 4-fluorobenzoic acid and trimesic acid (TMA) in water (Scheme S1) to further demonstrate that carboxylic acids chemisorb onto the surface. One fluorine signal is observed at 686.9 eV indicating deposition of 4-fluorobenzoic acid onto ceria. The C1s spectrum (Fig. S26) were fitted with four peaks appearing at 293, 288.3, 287, and 284.4 eV (FWHM = 1.55). The peak at 287 eV appears in the region for COOH carbons and aromatic carbons appearing at 284.4 eV overlap with adventitious carbon. The O 1s peaks at 532.6 and 530.9 eV (FWHM = 1.43) appear in the region for C=O and C-O species, respectively, and confirm binding of 4-fluorobenzoic acid to surface.

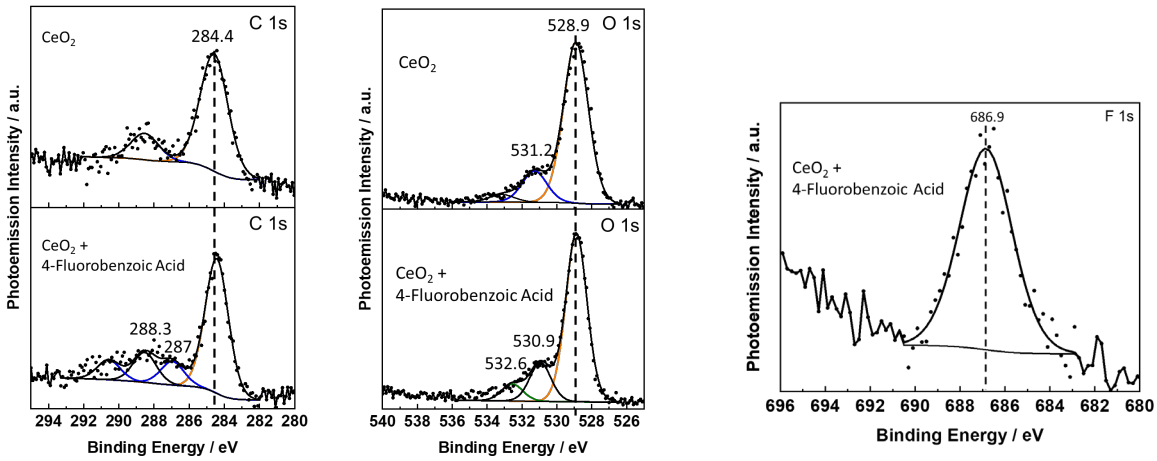

Fig. S26 O 1s (left) and C 1s (right) XPS spectra for CeO_2 (top) and 4-fluorobenzoic acid + CeO_2 (bottom) and F 1s XPS spectrum of reaction of 4-fluorobenzoic acid + CeO_2 (right).

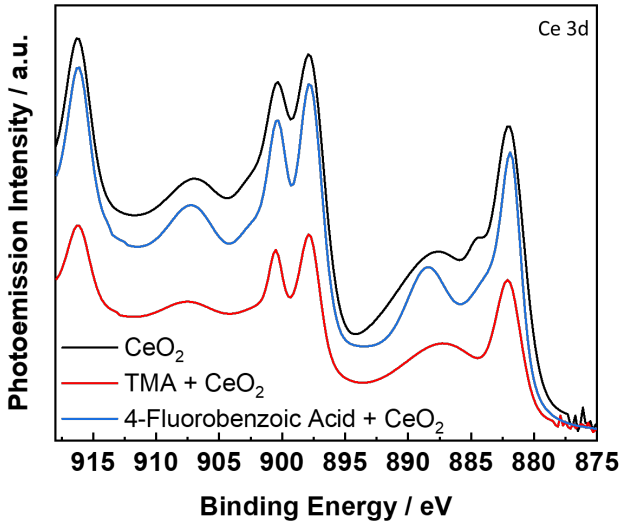

Fig. S27 Ce 3d XPS spectra (left) of CeO_2 (black), TMA + CeO_2 (red), and 4-fluorobenzoic acid + CeO_2 (blue).

The Ce 3d peaks for ceria treated with TMA are lower in intensity compared to ceria and ceria treated with 4-fluorobenzoic acid, suggesting higher surface coverage with TMA (Fig. S27). This is further supported by the higher peak intensity in O 1s and C 1s for TMA + CeO_2 versus CeO_2. The O 1s peak for CeO_2 + TMA (Fig. S28) is fitted with two peaks at 532.6 and 531.2 eV (FWHM = 1.44; intensities ~1:1) for C=O and C-O of carboxylate oxygens. These are shifted from O 1s peaks at 533.2 and 531.8 eV (FWHM = 1.56) for pure solid TMA to suggest that TMA has bound to the surface. The C 1s spectrum for CeO_2 + TMA is shows a peak at 288.3 eV (FWHM = 1.45) that is present for TMA (FWHM = 1.22) but absent for CeO_2, further indicating that TMA has absorbed

onto the surface. The larger FWHM in C1s for TMA on CeO_2 is consistent with carboxylic and aromatic carbons being in different chemical environments on the surface.

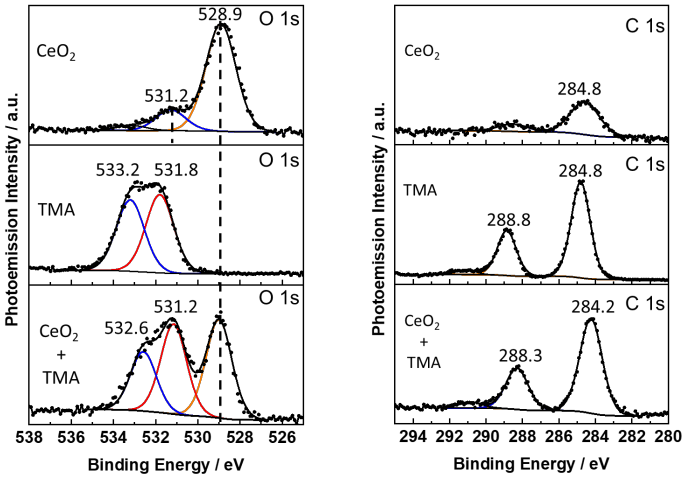

Fig. S28 O 1s (left) and C 1s (right) XPS spectra for CeO_2 (top), pure solid TMA (middle), and reaction of CeO_2 + TMA.

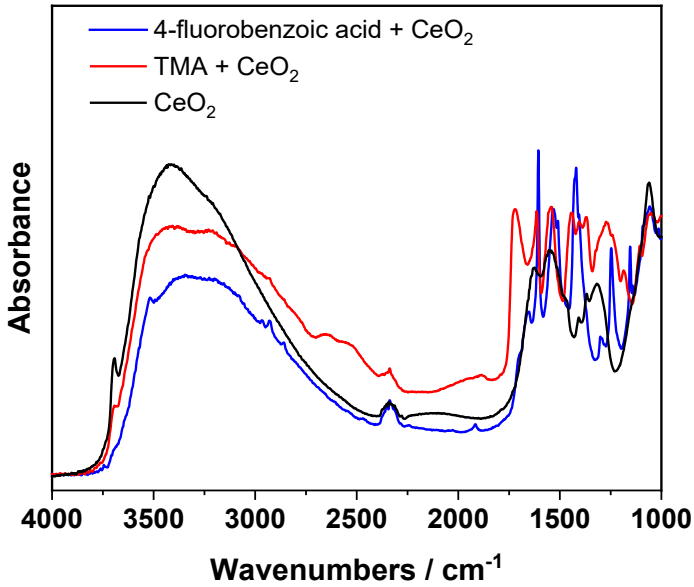

Fig. S29 DRIFTS spectra of CeO_2 (black), TMA + CeO_2 (red), and 4-fluorobenzoic acid + CeO_2 (blue).

EXAFS data for Pt/Ligand/CeO_2 before and after catalysis when Ligand is PDO and PDO-C

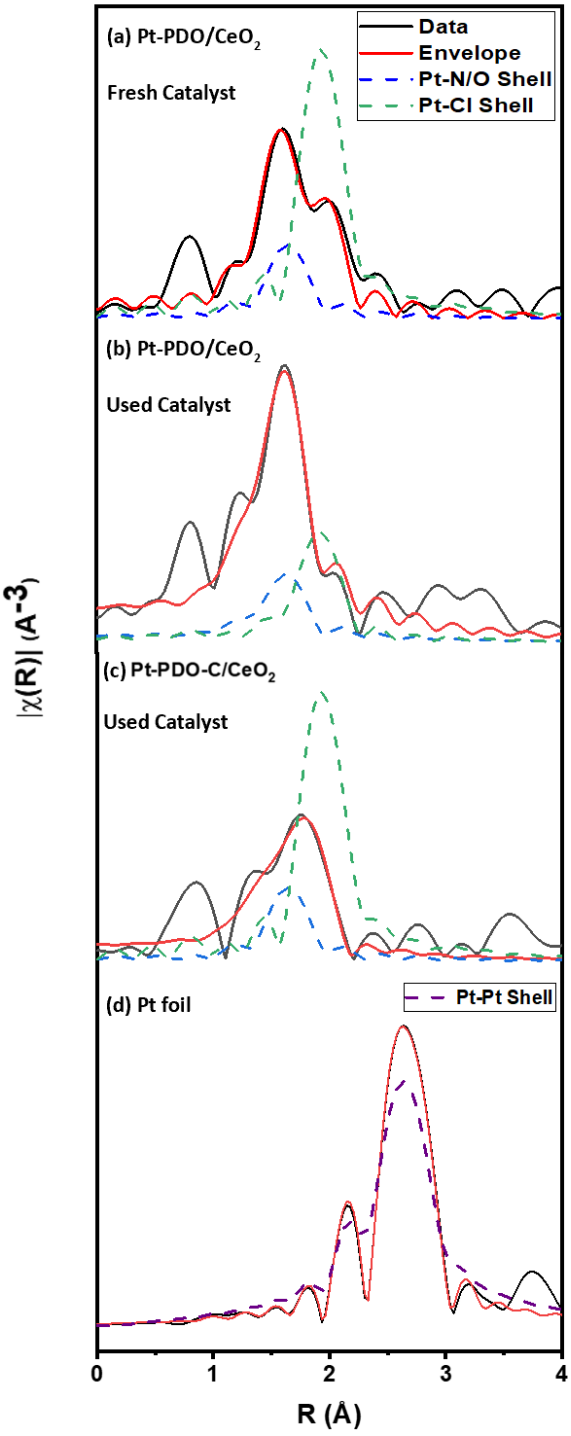

Fig. S30 EXAFS data with fitting envelopes for (a) Pt-PDO/CeO_2 fresh catalyst, (b) Pt-PDO/CeO_2 used catalyst, (c) Pt-PDO-C/CeO_2 used catalyst, and (d) Pt foil.

Table S4 EXAFS analysis for Pt-Cl and Pt-O/N coordination number in samples Pt-PDO/CeO_2 fresh, Pt-PDO/CeO_2 used and Pt-PDO-C/CeO_2 used catalysts. Fitting shown in Fig. S30.

Catalyst	Pt-Cl		Pt-O/N	
Pt-PDO/CeO_2 Fresh	***N***	***R (Å)***	***N***	***R (Å)***
	1.08 (± 0.45)	2.31(± 0.01)	3.96 (± 0.68)	2.01 (± 0.01)
Pt-PDO/CeO_2 Used	0.017 (± 0.11)	2.36 (± 0.07)	5.88 (± 0.99)	2.01 (± 0.01)
Pt-PDO-C/CeO_2 Used	1.32 (± 1.68)	2.26 (± 0.04)	6.89 (± 3.41)	2.07 (± 0.05)

In addition to the fitting shown above, we repeated EXAFS fitting with the inclusion of the Pt-Pt path to demonstrate that there is virtually no Pt-Pt scattering detected in either catalyst after reaction (Fig. S31 and Table S5).

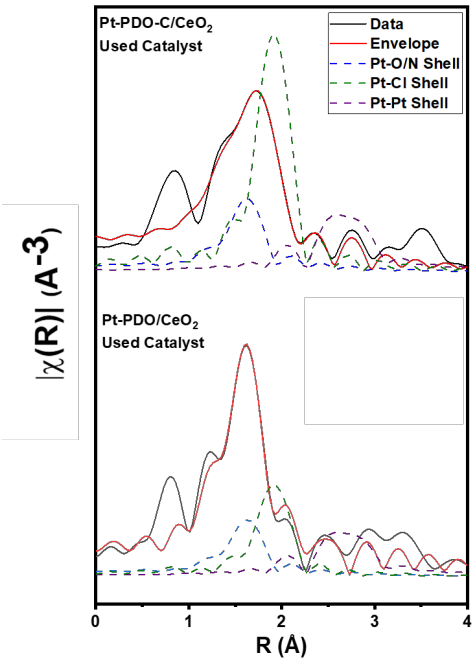

Fig. S31 Fitting of Pt-PDO-C/CeO_2 used catalyst and Pt-PDO/CeO_2 used catalyst with Pt-Pt path included in fitting.

Table S5 EXAFS analysis for Pt-Pt, Pt-Cl, and Pt-O/N coordination number in samples Pt-PDO/CeO_2 used and Pt-PDO-C/CeO_2 used catalysts. Fitting shown in Fig. S31.

Catalyst	Pt-Pt		Pt-Cl		Pt-O/N	
Pt-PDO-C/CeO_2 Used	*N*	*R (Å)*	*N*	*R (Å)*	*N*	*R (Å)*
	0.12 (± 0.35)	2.78 (± 0.01)	0.94 (± 1.04)	2.26 (± 0.04)	6.76 (± 2.66)	2.01 (± 0.01)
Pt-PDO/CeO_2 Used	-0.01 (± 0.08)	2.78 (± 0.03)	0.01 (± 0.01)	2.33 (± 0.04)	6.20 (± 1.03)	2.01 (± 0.01)

Hydrosilylation Yields for Pt/Ligand/CeO_2, where Ligand = PDO, PDO-C, and PDO-C2

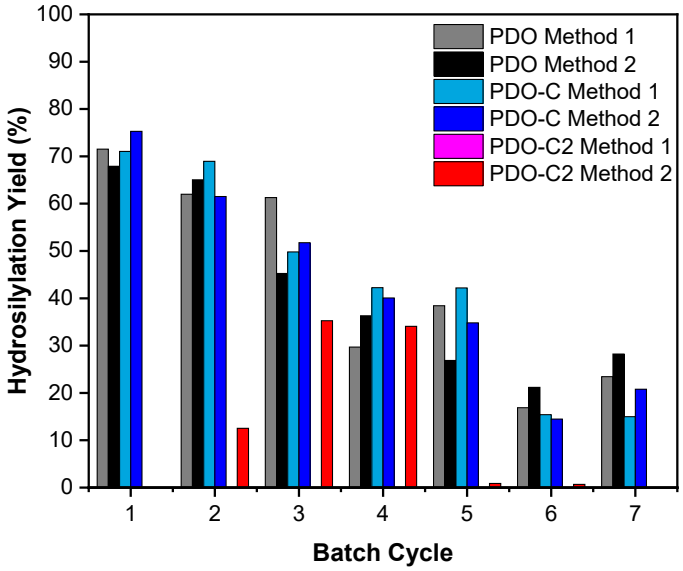

Fig. S32 Comparison of hydrosilylation yields for seven consecutive runs using six heterogeneous catalysts Pt(II)/Ligand/CeO_2, where L = PDO (gray and black), PDO-C (light blue and blue), and PDO-C2 (pink and red) prepared by synthetic methods 1 and 2.

Representative GC/MS chromatogram of hydrosilylation reactions

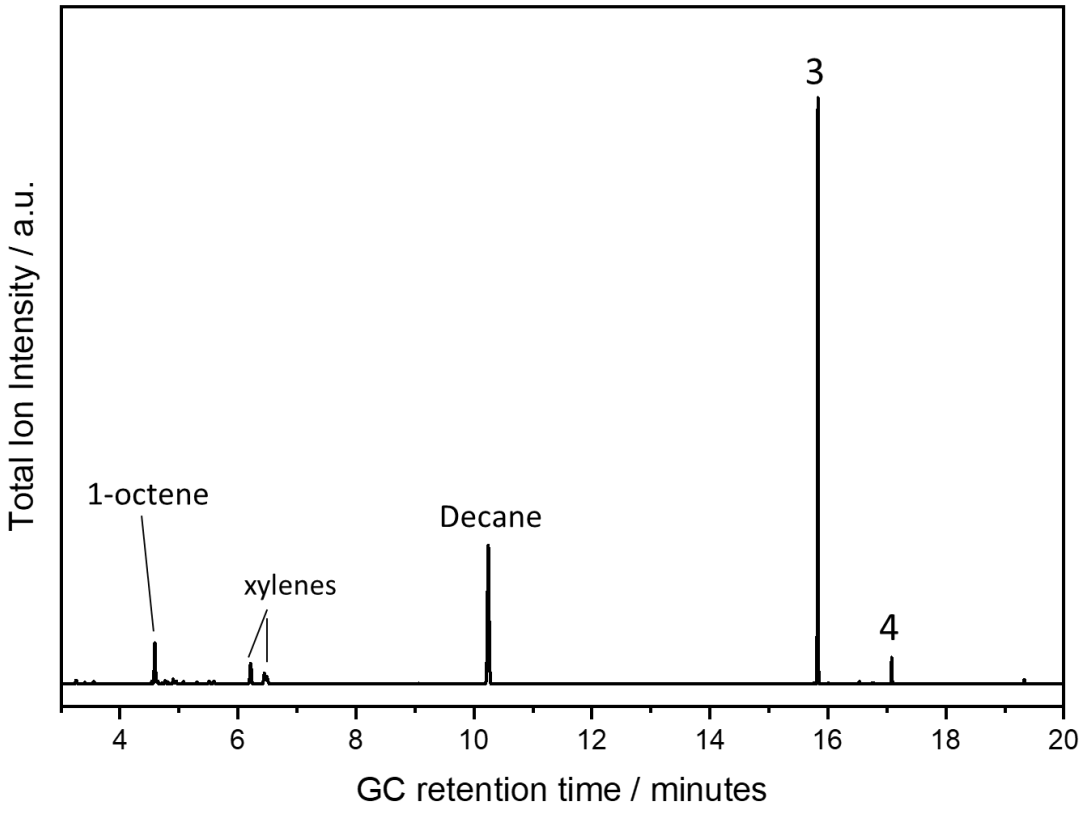

Fig. S33 TIC of hydrosilylation reaction using Pt-PDO/CeO_2 representative for all hydrosilylation reactions using catalysts Pt-Ligand/CeO_2, where Ligand = PDO, PDO-C, and PDO-C2 prepared using synthetic methods 1 and 2. Decane is internal intensity standard.

XPS and DRIFTS spectra of SAC before and after 8 cycles of catalysis

Fig. S34-S44 are a comparison of XPS and DRIFTS spectra of Pt/Ligand/CeO_2, where Ligand is PDO, PDO-C, and PDO-C2, before and after 8 cycles of catalysis to show the loss of SAC and buildup of silane on ceria surface.

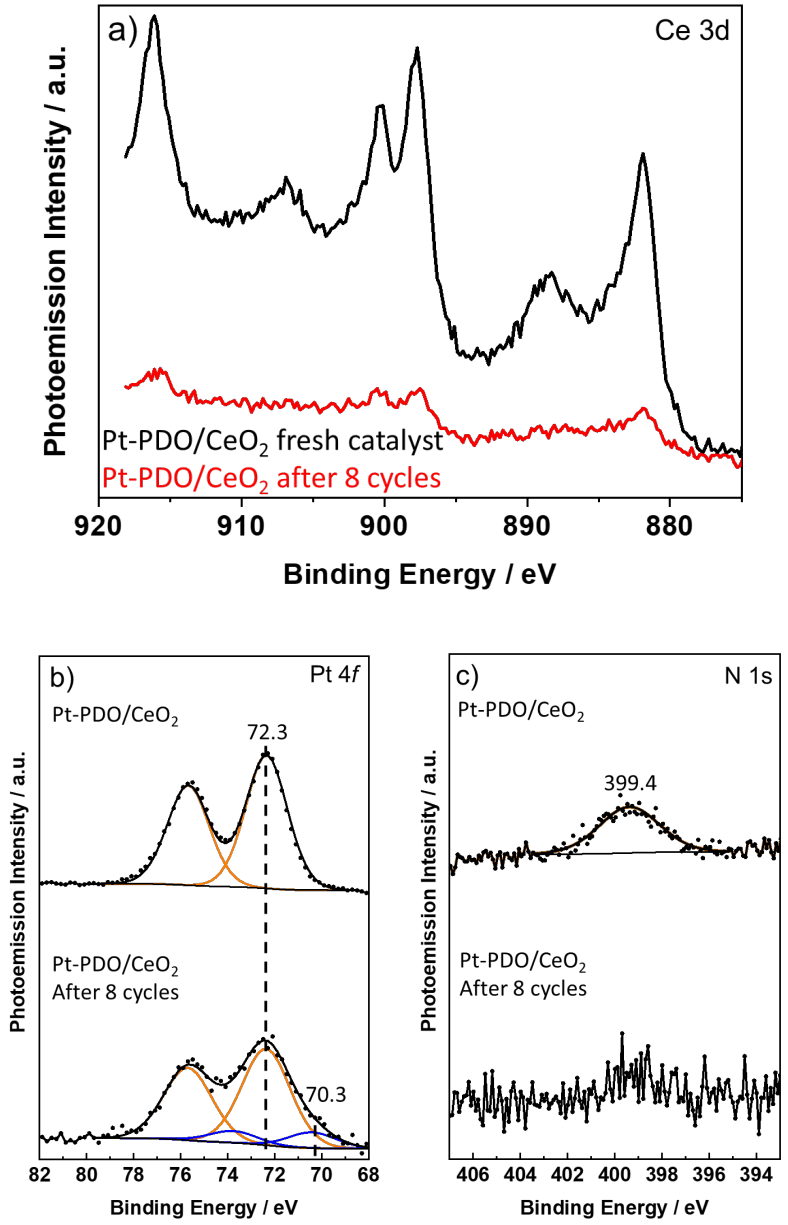

Fig. S34 a) Ce 3d XPS spectra of Pt-PDO/CeO_2 before (black) and after 8 cycles of hydrosilylation (red). Stacked Pt 4f (b) and N 1s (c) XPS spectra of Pt-PDO/CeO_2 before (top) and after 8 cycles of hydrosilylation (bottom).

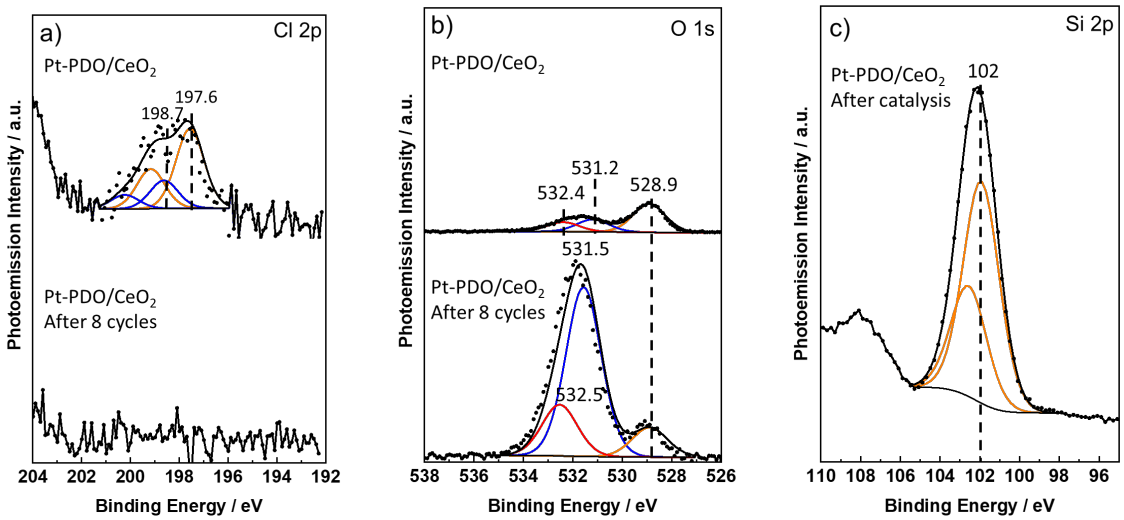

Fig. S35 Cl 2p (a) and O 1s (b) XPS spectra of Pt-PDO/CeO_2 before (top) and after 8 cycles of hydrosilylation (bottom), and Si 2p (c) XPS spectra of Pt-PDO/CeO_2 after 8 cycles of hydrosilylation.

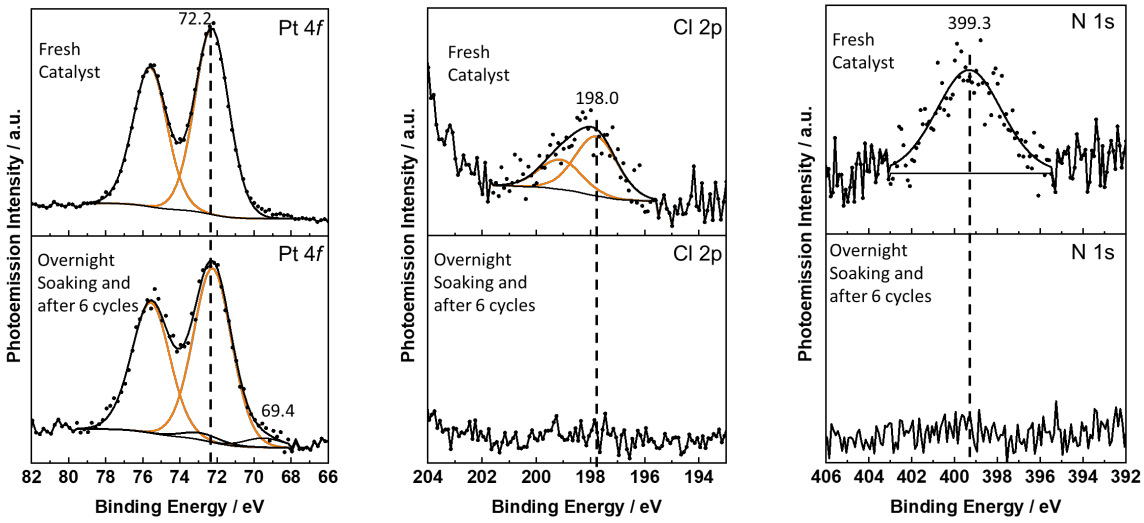

Fig. S36 Pt4f (left), Cl2p (middle), and N1s (right) XPS spectra for fresh catalyst Pt-PDO/CeO_2 (top) versus after soaking overnight in toluene for six runs (bottom) without normalization by Ce3d peak height showing that even with overnight soaking the peak intensities for Pt 4f, Cl 2p, and N1s decrease; such soaking does not wash away the silane deposit.

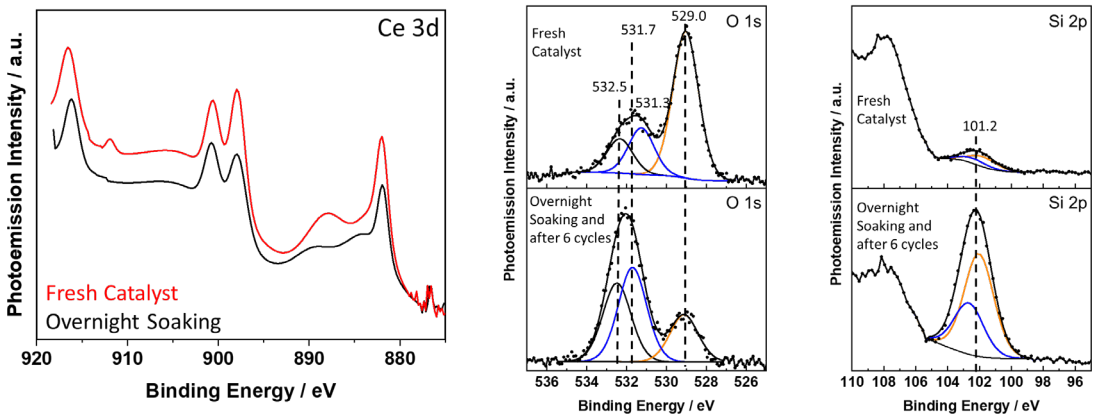

Fig. S37 Ce 3d XPS spectra on left. Stacked O 1s (middle), Si 2p (right) XPS spectra for fresh catalyst Pt-PDO/CeO_2 (top) versus after soaking overnight in toluene for six runs (bottom) without normalization with Ce3d peak height. The Ce 3d peak intensity still decreases and O 1s and Si 2p peaks increase with successive runs, demonstrating that the overnight soaking isn't improving yields.

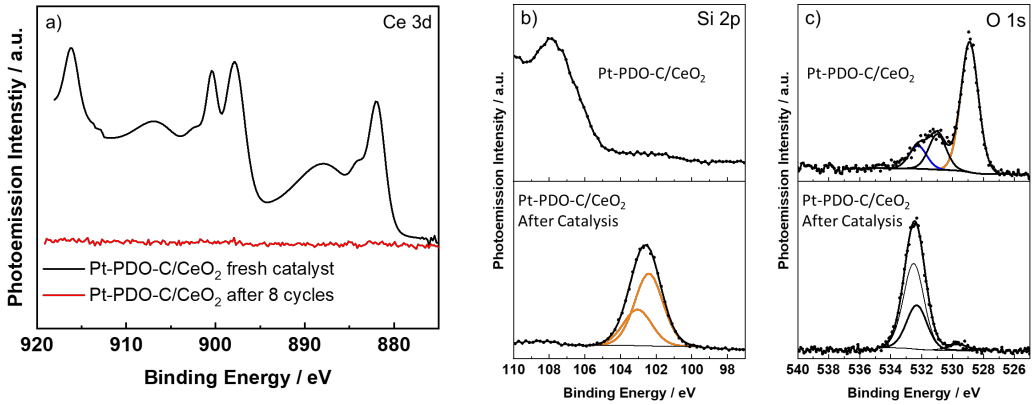

Fig. S38 Ce 3d XPS spectra before (black) and after catalysis (red) and stacked Si 2p and O 1s XPS spectra of Pt-PDO-C/CeO_2 before (top) and Pt-PDO-C/CeO_2 after (bottom) catalysis. Increase in O 1s and Si 2p peaks and decrease in Ce 3d peaks show silane buildup after successive batch cycles.

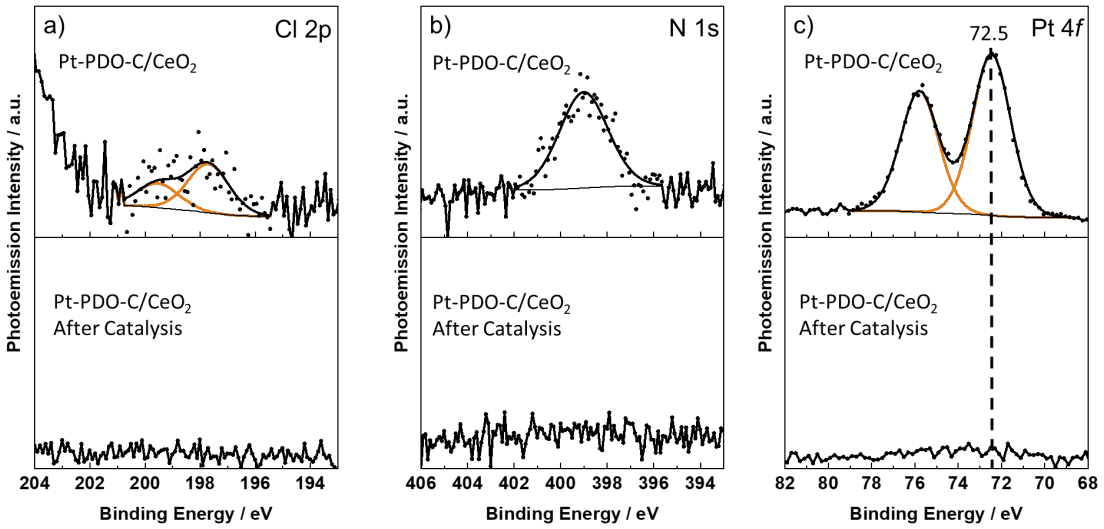

Fig. S39 Cl 2p (a), N 1s (b), and Pt 4f (c) XPS spectra of Pt-PDO-C/CeO_2 before (top) and Pt-PDO-C/CeO_2 after eight batch cycles (bottom).

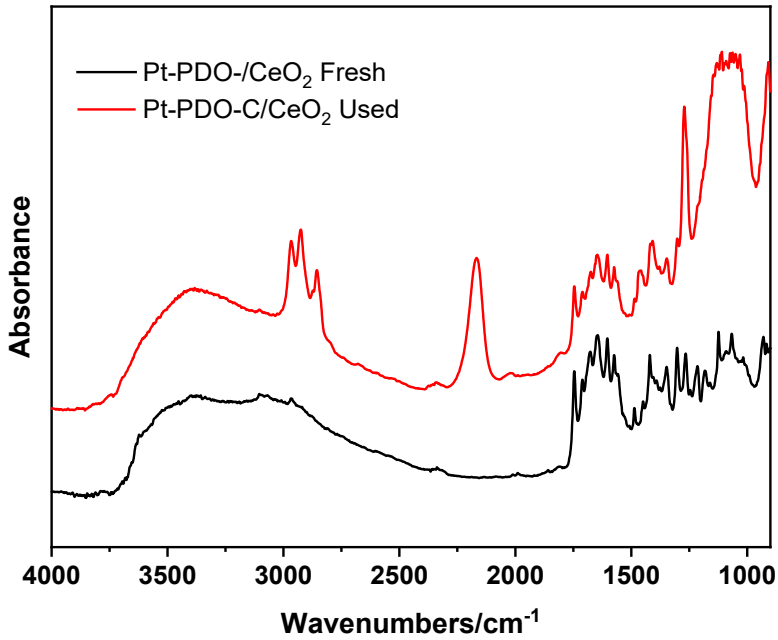

Fig. S40 DRIFT spectra for Pt-PDO-C/CeO_2 fresh (black) and Pt-PDO-C/CeO_2 used (red) catalysts shows that $HSi(OMe)_2Me$ is depositing on surface.

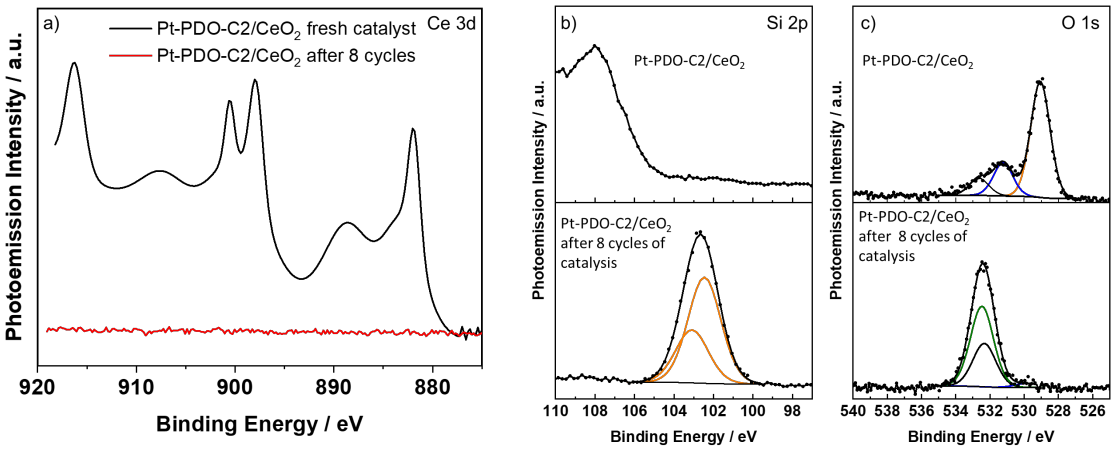

Fig. S41 Ce 3d XPS spectra before (black) and after catalysis (red) and stacked Si 2p and O 1s XPS spectra of Pt-PDO-C2/CeO_2 before (top) and Pt-PDO-C2/CeO_2 after (bottom) catalysis. Increase in O 1s and Si 2p peaks and decrease in Ce 3d peaks show silane buildup after successive batch cycles.

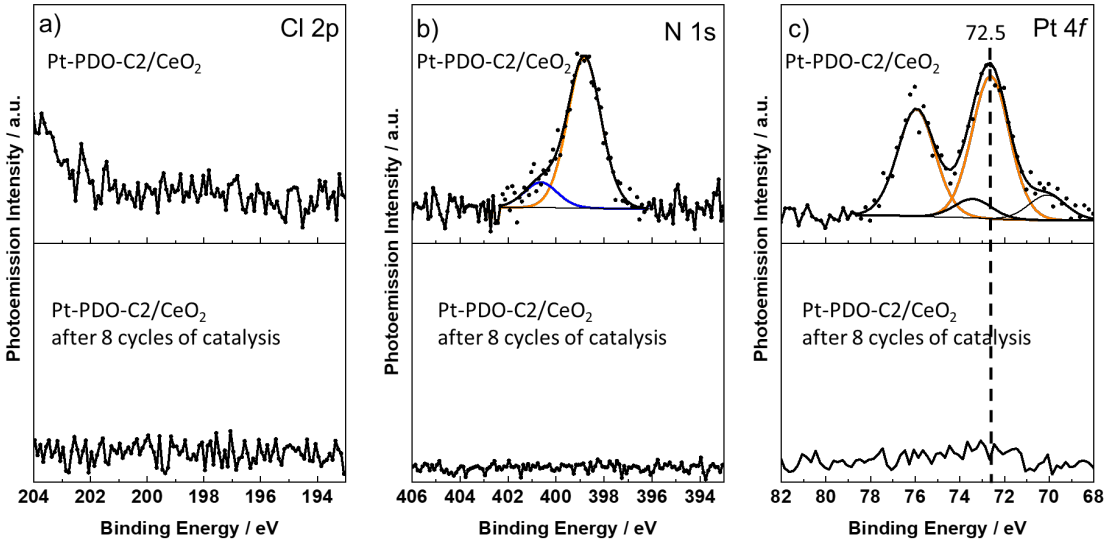

Fig. S42 Cl 2p (a), N 1s (b), and Pt 4f (c) XPS spectra of Pt-PDO-C2/CeO_2 before (top) and Pt-PDO-C2/CeO_2 after eight batch cycles (bottom).

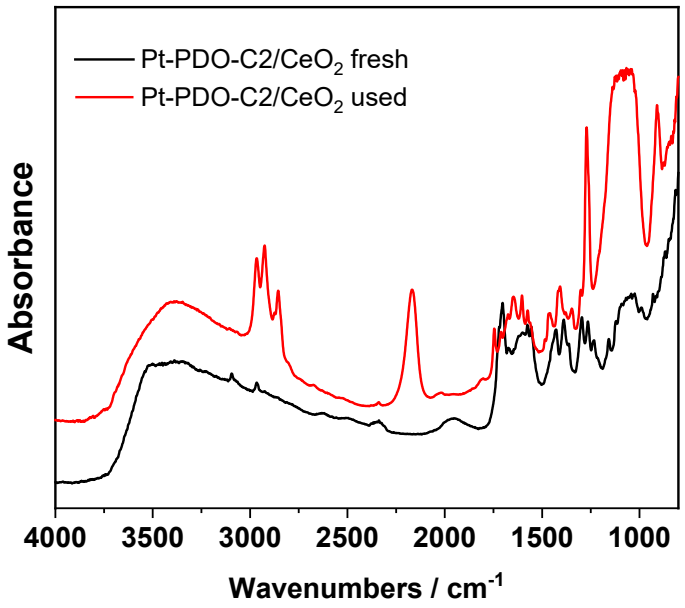

Fig. S43 DRIFTS spectra for Pt-PDO-C2/CeO_2 fresh (black) and Pt-PDO-C2/CeO_2 used (red) catalysts.

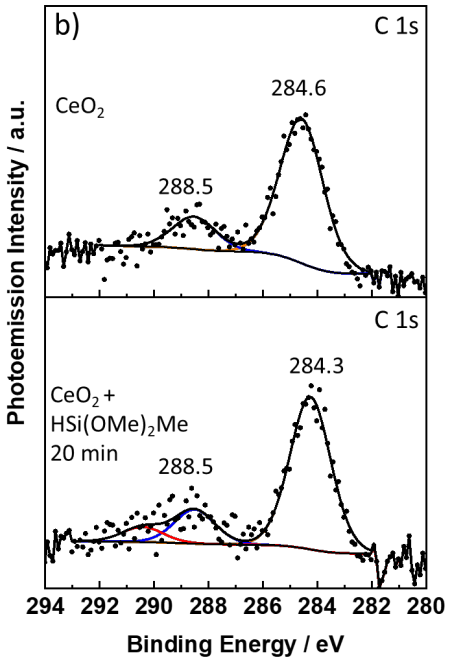

Fig. S44 Si 2p (a) and C 1s (b) XPS spectra for CeO_2 (top) and CeO_2 exposed to $HSi(OMe)_2Me$ for 20 minutes at 70 °C in toluene (bottom).

Silane Buildup on CeO_2 Increases with Exposure Time

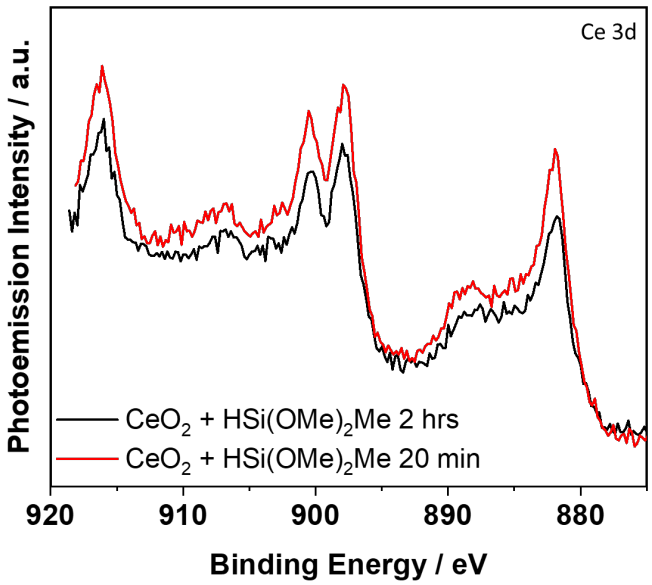

Fig. S45 Ce 3d XPS spectra of CeO_2 + $HSi(OMe)_2Me$ heated in toluene for 20 minutes (red) and 2 hours (black).

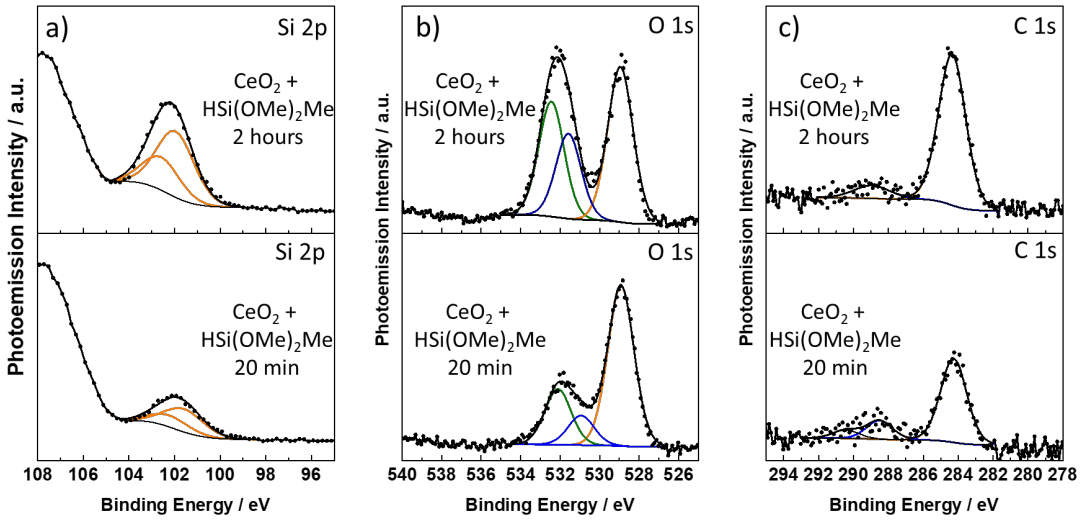

Fig. S46 Si 2p (a), O 1s (b), and C 1s (c) for CeO_2 + $HSi(OMe)_2Me$ heated for 20 minutes (bottom) and 2 hours (top).

Calculation of silane coverage on ceria surface

Calculation to estimate thickness of silane buildup on ceria surface.

Equation S1 is the attenuation of XPS signal due to an overlayer:

Formula is I / I0 = exp(– d / lambda * cos theta), theta is 45 degrees

Before reaction: 5883.33 cps – 2938.68 cps = 2944.65 cps

After reaction: 5332.14 cps – 2938.68 cps = 2393.46 cps

I/I0 = 0.8128

d = – lambda * cos theta * ln (I/I0)

1.5 - 2.2 nm

Testing Silicon Heteroatom substituent for reactivity towards CeO_2: proving surface silylation

Taking advantage of the known reactivity of silanes containing hydrolysable groups, the silanes Me_3SiCl, Me_2SiCl_2, and $PhSi(OMe)_3$ were explored first (before catalysis) to coat reactive sites to prevent later reaction of $HSi(OMe)_2Me$ with surface (add to after catalysis section). Silylation of surface with Me_3SiCl and Me_2SiCl_2 were accomplished by exposing the ceria to an atmosphere of the silane under static vacuum, while the less volatile $HSi(OMe)_2Me$ and $PhSi(OMe)_3$ were heated at 70 °C for 2-12 hours with ceria in toluene.

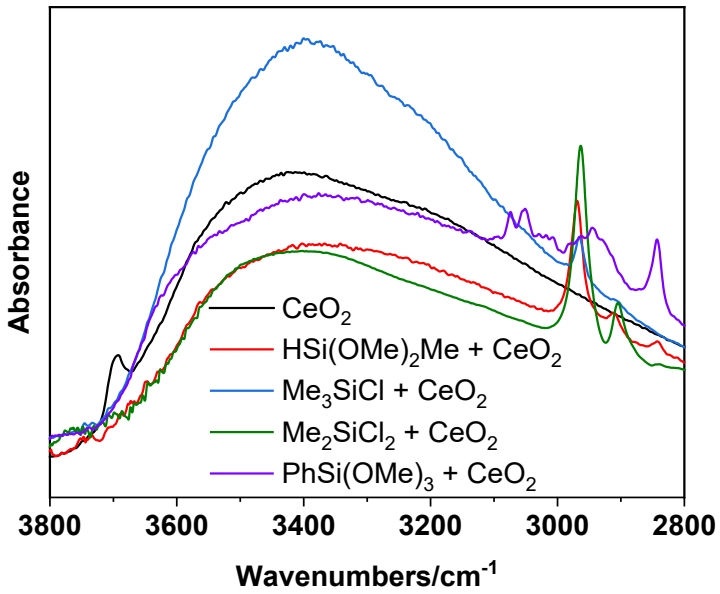

Fig. S47 DRIFT spectra from 4000 – 2500 cm^{-1} of ceria treated with $HSi(OMe)_2Me$ (red), Me_3SiCl (blue), Me_2SiCl_2 (green), and $PhSi(OMe)_3$ (lavender).

The overlaid DRIFTS spectra (Fig. S47) shows that all of the silanes react with the terminal hydroxy group on ceria surface (3700 cm^{-1}). The peak at 2962 cm^{-1} corresponds to C-H stretch of CH_3 of $H\text{-}Si(OMe)_2Me$, Me_3SiCl, and Me_2SiCl_2 that have chemisorbed to the surface. The peak at 3055 cm^{-1} is a C-H stretch from phenyl and the peaks from 2000-1780 cm^{-1} are overtones from phenyl group indicating that $PhSi(OMe)_3$ has chemisorbed.

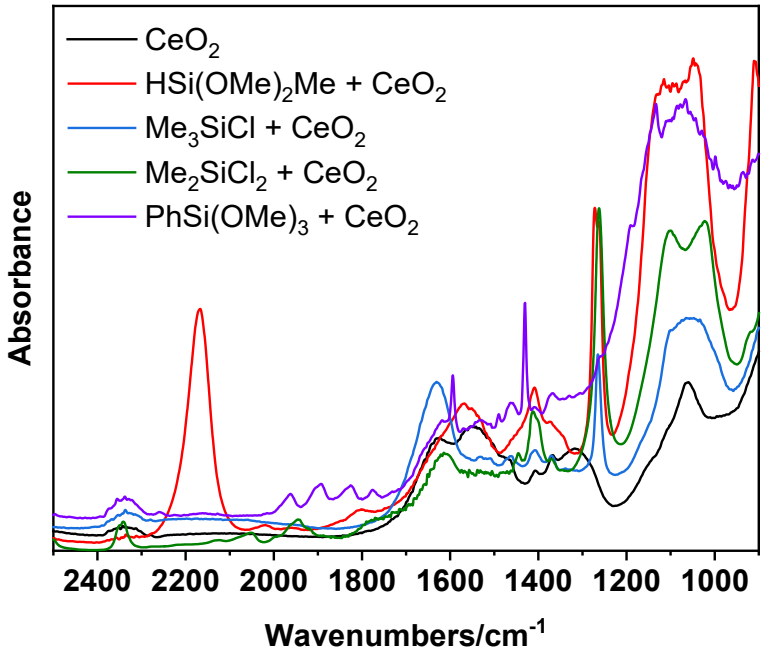

Fig. S48 DRIFTS spectra from 2500 – 900 cm^{-1} of ceria treated with $HSi(OMe)_2Me$ (red), Me_3SiCl (blue), Me_2SiCl_2 (green), and $PhSi(OMe)_3$ (lavender).

The assignments of peaks from region 1500-1000 cm^{-1} and peak at 2165 cm^{-1} have been discussed above but comparison of spectra in Figure S48 yields important information on reactivity of silane. The silanes Me_3SiCl and Me_2SiCl_2 that chemisorbed onto the surface do not contain methoxy groups, which explains the absence of a peak around 910 cm^{-1} that is observed when ceria is treated with $HSi(OMe)_2Me$, which is also absent when ceria is treated with $PhSi(OMe)_3$ (see below for explanation).

The appearance of peaks in the region from 1115-1048 cm^{-1} indicates Si-O and Si-O-Si stretches. The intensity of the peak at 1262 cm^{-1} versus 1115 cm^{-1} is much higher for Me_2SiCl_2 than for $HSi(OMe)_2Me$, which is consistent with more methyl groups. For $PhSi(OMe)_3$, the peaks at 1115-1048 cm^{-1} are present to indicate Si-O-Si and Si-O bonds on surface.

When CeO_2 is exposed to Me_3SiCl the Ce 3d (Fig. S49) and C 1s peaks (Fig. S53) show very little change in intensity from CeO_2, and a very weak peak in the Si 2p spectrum is observed (Fig. S50). The corresponding Cl 2p spectrum (Figure S52) shows the buildup of chloride, suggesting that the silylated product may be hydrolyzed during workup.

In contrast, Me_2SiCl_2 deposits very little chloride on the surface, and shows the lowest Ce 3d, Si 2p, and O 1s peak intensities for ceria exposed to silane, indicating highest surface coverage. The O1s spectrum is similar to CeO_2 + $HSi(OMe)_2Me$, where two components are fitted for the peak at 532 eV. Since Me_2SiCl_2 doesn't introduce oxygen, the fitted peaks for the two new O1s peaks must be derived from the surface. The Si2p peak for CeO_2 + Me_2SiCl_2 is higher in peak intensity than Me_3SiCl but comparable to $HSi(OMe)_2Me$. $HSi(OMe)_2Me$ and $PhSi(OMe)_3$ required elevated temperatures to bind to the surface, while Me_2SiCl_2 and Me_3SiCl vapors reacted with ceria surface at room temperature. This implies that silanes with chlorides are more reactive than silanes with methoxy groups towards ceria.

The low intensity of the Si 2p peak for ceria exposed to $PhSi(OMe)_3$ indicates it is not easily deposited on the surface. The absence of a peak at 3700 cm^{-1} (Figure S47) shows that the terminal hydroxy groups on ceria are gone and the absence of a peak at 1272 cm^{-1} indicates that all of the methoxy groups of $PhSi(OMe)_3$ chemisorbed onto the surface have been hydrolyzed; therefore, the fitted peak at 530 eV (Figure S48) is a new oxygen species on ceria. With evidence indicating the methoxy groups have been completely hydrolyzed, the presence of two new O 1s peaks at 530 and 531.7 eV must be a combination of Si-O-Si and Si-O-Ce on the surface.

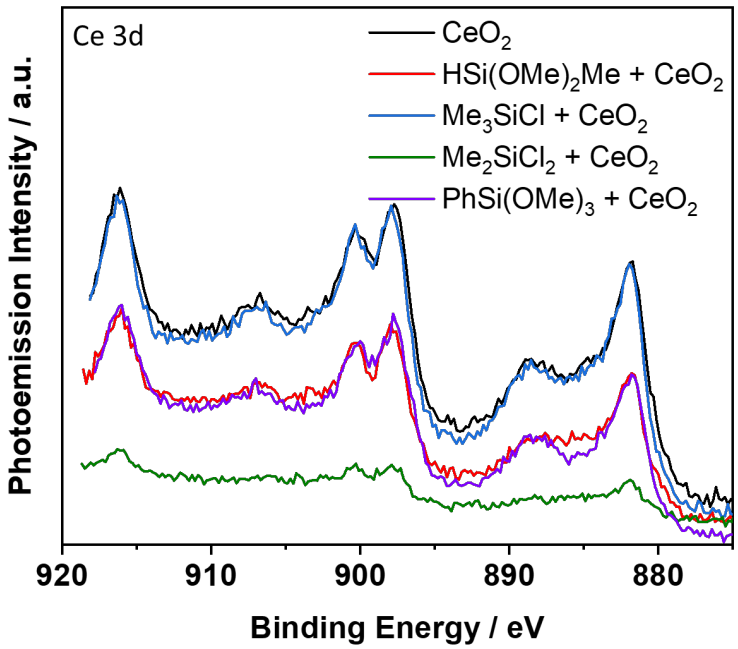

Fig. S49 Ce 3d XPS spectra of ceria exposed to $HSi(OMe)_2Me$ (red), Me_3SiCl (blue), Me_2SiCl_2 (green), and $PhSi(OMe)_3$ (lavender).

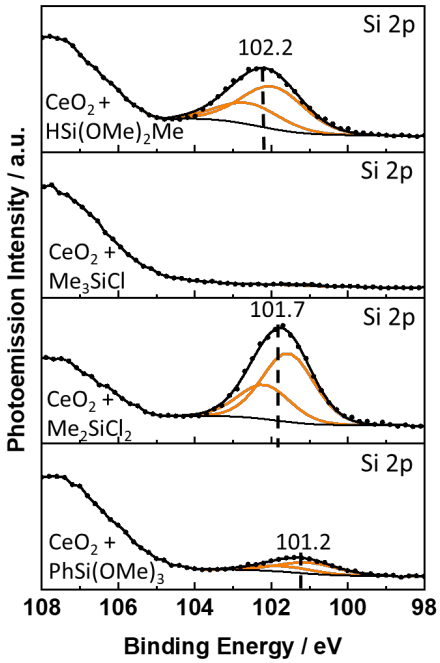

Fig. S50 Si 2p XPS spectra of CeO_2 and CeO_2 exposed to $HSi(OMe)_2Me$, Me_3SiCl, Me_2SiCl_2, and $PhSi(OMe)_3$ (top to bottom).

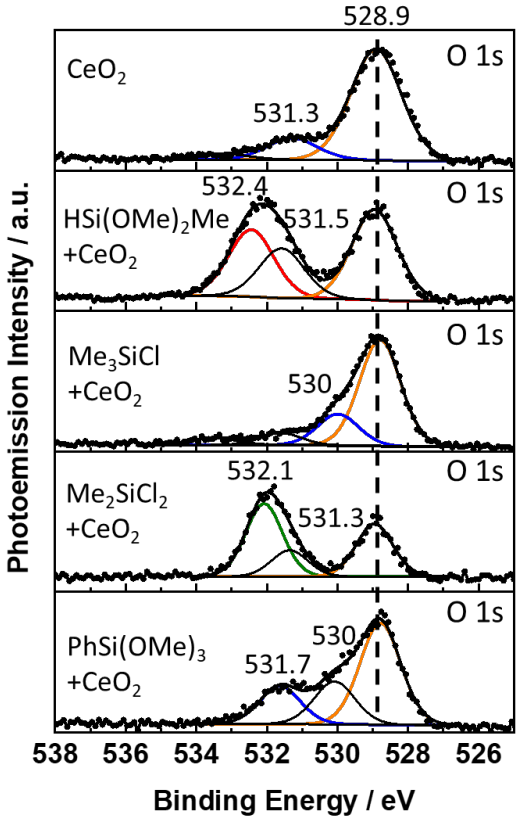

Fig. S51 O 1s XPS spectra of CeO_2 and CeO_2 exposed to $HSi(OMe)_2Me$, Me_3SiCl, Me_2SiCl_2, and $PhSi(OMe)_3$ (top to bottom).

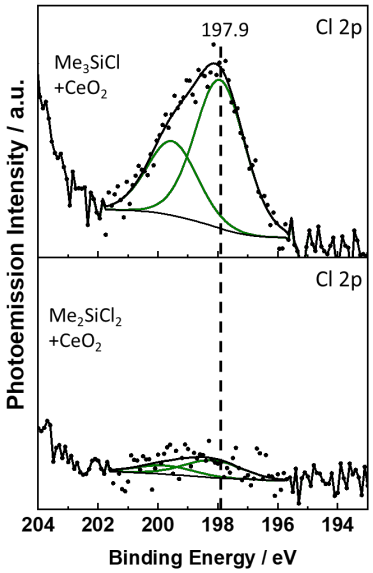

Fig. S52 Cl 2p XPS spectra for CeO_2 exposed to Me_3SiCl (top) and Me_2SiCl_2 (bottom).

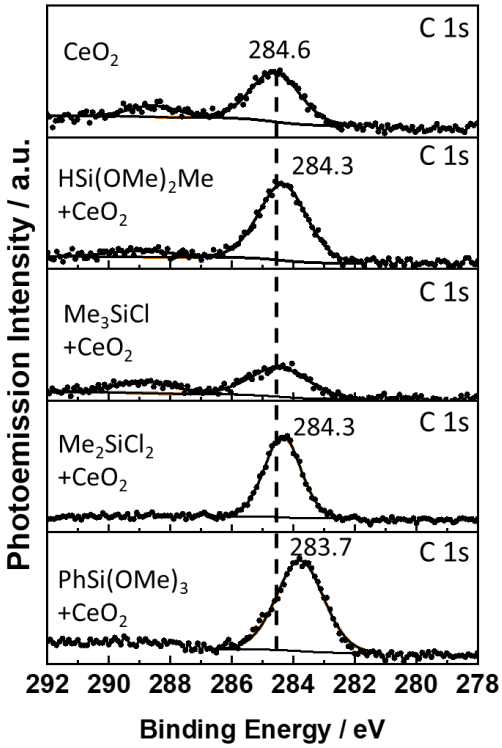

Fig. S53 C 1s XPS spectra of CeO_2 and CeO_2 exposed to $HSi(OMe)_2Me$, Me_3SiCl, Me_2SiCl_2, and $PhSi(OMe)_3$ (top to bottom).

CO Adsorption Experiment to Probe Pt Species on Ceria

CO adsorption experiments were performed with a diffuse reflectance IR environmental chamber (PIKE Technologies, 162-4160, HTV). Background spectra were collected under Ar flow before purging the chamber with 10% CO in Ar. After CO flowed into the chamber for 15 minutes, the chamber was purged with pure Ar for 15 minutes to remove gas-phase CO, as well as weakly adsorbed CO from the catalyst surface. Diffuse reflectance infrared Fourier transform spectra (DRIFTS) were collected with a Magna 550 FTIR spectrometer. Each DRIFT spectrum was an average of 500 scans and was converted into Kubelka-Munk units.

As seen from Fig. S54, there is a sharp peak at 2094 cm^{-1} on Pt-PDO/CeO_2 single atom catalyst at 70 °C which is attributed to CO adsorbed on positively charged Pt single sites.[10] In addition, there are not any peaks at lower wavenumbers (~2040-2080 cm^{-1}) and ~1800 cm^{-1} which would be attributed to linear and bridge-bonded CO on metallic Pt sites, respectively. This indicates that Pt NPs are not present in this catalyst. We note that CO adsorption is not observed at 30 °C, but is indicated at 70 °C. This is due to the presence of chlorine ligands coordinated to the Pt single atoms (Table 1). By increasing the temperature, chlorine ligands have been removed and CO adsorbs on the Pt single sites.

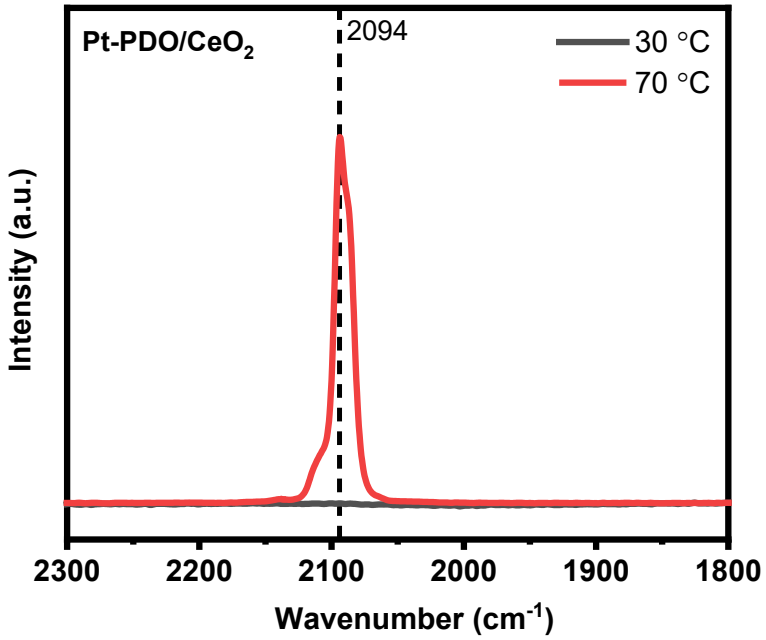

Fig. S54 DRIFTS spectrum of Pt-PDO/CeO_2 exposed to 10% CO in Ar at 70 °C

References

1. Baraldi, A.; Dhanak, V. R., Design Study Of A Double-Pass Hemispherical Electron-Energy Analyzer With Multichannel Detection. *Journal Of Electron Spectroscopy And Related Phenomena* **1994,** *67* (1), 211-220.

2. Krause, L.; Herbst-Irmer, R.; Sheldrick, G. M.; Stalke, D., Comparison of silver and molybdenum microfocus X-ray sources for single-crystal structure determination. *J. Appl. Crystallogr.* **2015,** *48* (1), 3-10.

3. Sheldrick, G., SHELXT - Integrated space-group and crystal-structure determination. *Acta Crystallogr. Sect. A: Found. Crystallogr.* **2015,** *A71* (1), 3-8.

4. Sheldrick, G., Crystal structure refinement with SHELXL. *Acta Crystallogr. Sect. C: Cryst. Struct. Commun.* **2015,** *71* (1), 3-8.

5. Falivene, L.; Cao, Z.; Petta, A.; Serra, L.; Poater, A.; Oliva, R.; Scarano, V.; Cavallo, L., Towards the online computer-aided design of catalytic pockets. *Nature Chemistry* **2019,** *11* (10), 872-879.

6. Roy, S.; Hagen, K. D.; Maheswari, P. U.; Lutz, M.; Spek, A. L.; Reedijk, J.; van Wezel, G. P., Phenanthroline Derivatives with Improved Selectivity as DNA-Targeting Anticancer or Antimicrobial Drugs. *ChemMedChem* **2008,** *3* (9), 1427-1434.

7. Jin, S.; Wen, M.-F.; Liu, L.-F.; Gao, M.-J.; Wu, J.-Z., Synthesis and supramolecular networks of 5,6-dioxo-1,10-phenanthroline-2,9-dicarboxylic acid dihydrate and its first coordination compound cis-diaquachlorido(5,6-dioxo-1,10-phenanthroline-2,9-dicarboxylic acid-κ4O2,N,N′,O9)manganese(II) chloride dihydrate. *Acta Crystallogr. Sect. C: Cryst. Struct. Commun.* **2012,** *68* (5), m135-m138.

8. Eckert, T. S.; Bruice, T. C., Chemical properties of phenanthrolinequinones and the mechanism of amine oxidation by o-quinones of medium redox potentials. *J. Am. Chem. Soc.* **1983,** *105* (13), 4431-4441.

9. Lei, Y.; Anson, F. C., Hydration of the Carbonyl Groups in 1,10-Phenanthroline-5,6-dione Induced by Binding Protons or Metal Cations to the Pyridine Nitrogen Sites. *J. Am. Chem. Soc.* **1995,** *117* (39), 9849-9854.

10. DeRita, L.; Dai, S.; Lopez-Zepeda, K.; Pham, N.; Graham, G. W.; Pan, X.; Christopher, P., Catalyst architecture for stable single atom dispersion enables site-specific spectroscopic and reactivity measurements of CO adsorbed to Pt atoms, oxidized Pt clusters, and metallic Pt clusters on TiO2. *Journal of the American Chemical Society* **2017,** *139* (40), 14150-14165.